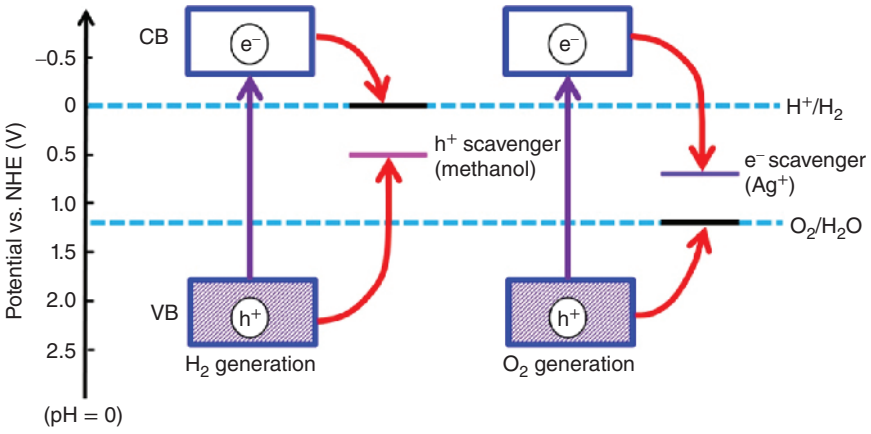

Figure 1.18 Photocatalytic H_2-generation and O_2-generation reactions in the presence of hole and electron sacrificial agents, respectively.

biomass energy, and its application value is obvious. In contrast, when Na_2S, K_2S, Na_2SO_3, $Na_2S_2O_4$, NaI, and KSCN are used as electron donors, even without any photocatalyst, HER will occur under UV irradiation [350]. Therefore, when we use these reductants as sacrificial agents for photocatalytic H_2 evolution, we should consider the photo-induced H_2 evolution behavior of these electron donors without photocatalyst. On the other hand, commonly used sacrificial agents for photocatalytic oxygen production reactions include Ag^+, Fe^{3+}, Ce^{4+}/Ce^{3+}, Fe^{3+}, $PtCl_2^-$, $AuCl_4^-$, $Na_2S_2O_8$, and $K_2S_2O_8$. Photogenerated electrons in the CB of semiconductor photocatalysts can be consumed by these oxidants in time, and the oxygen production reaction can be enhanced. However, it should be noted that although some oxidants (such as Ag^+) have a suitable oxidation potential, the reduced products (e.g. elemental Ag) may not be water soluble, which is deposited on the surface of the photocatalyst particles, hindering the light absorption, thus reducing the rate of OER and finally terminating the reaction. Therefore, it is generally observed that in the half-reaction system containing Ag^+, the oxygen production activity will gradually decrease over reaction time [34]. These reactions using sacrificial agents can be performed to evaluate whether a particular photocatalyst meets the thermodynamic and kinetic requirements for photocatalytic H_2 or O_2 production. However, even though a photocatalyst shows an activity of producing H_2 and O_2 in these reactions, the result does not guarantee that the photocatalyst has the activity for overall water splitting without a sacrificing agent. From this point of view, the term "water decomposition" should be treated differently from the hydrogen and oxygen production reactions in the presence of sacrificial agents. Water decomposition means that water can be completely decomposed to produce H_2 and O_2 at the stoichiometric ratio when there is no sacrificial agent. Additionally, for the specific half-reaction photocatalytic hydrogen production system, different sacrificial agents often have different H_2 production effects. For example, the photocatalytic H_2 production activity of g-C_3N_4 in the

presence of triethanolamine as sacrificial agent is significantly higher than that observed using CH_3OH, ethanol, or EDTA as sacrificial agent [59]. Therefore, for a specific system, we should pay attention to optimize the type and concentration of sacrificial agents.

1.5.1.2 Photocatalytic CO_2 Reduction

The rapid consumption of fossil energy has led to the increase of CO_2 concentration in the atmosphere year by year, which has caused global warming and energy shortage problems. Therefore, reducing CO_2 emissions and sustainably transforming CO_2 have become hot spots for both alleviating environmental pressure and realizing the recycling of carbon resources. From the chemical point of view, the stable CO_2 molecules with standard formation heat of $-394.38\,kJ\,mol^{-1}$ are inert, thus making its chemical fixation and transformation very difficult. In the process of CO_2 reduction, H_2O is generally selected as the best hydrogen source and electron donor species.

Thermodynamically speaking, HCHO, HCOOH, CH_3OH, and CH_4 are the simplest products of CO_2 reduction by H_2O through the uphill reactions (see Table 1.4), due to the positive Gibbs free energy ΔG^0 of these reactions. These uphill reactions are obviously different from several spontaneous downhill CO_2 hydrogenation reactions (to CH_3OH, CH_4, and low carbon olefins; see Table 1.5) with negative ΔG^0 values. Therefore, a large amount of energy must be input to convert CO_2 and H_2O into different organic molecules. Among various facile technologies, photocatalytic CO_2 reduction has been considered as the most promising CO_2 conversion technology, which could convert abundant and renewable solar energy, water, and CO_2 into useful organic fuels without consuming auxiliary energy in the reaction process, thus effectively reducing the CO_2 emission into the atmosphere. Therefore, through artificial photosynthesis, solar fuels, such as alkanes, alkenes, and alcohols, and other organic substances could be obtained by abiotic reduction under the sunlight, thus truly realizing the recycling of the carbon element.

At present, due to the difficulty in achieving the half reaction of O_2 evolution, current studies mainly focus on the half reaction of CO_2 reduction through introducing the proper sacrificial agents to consume photogenerated holes. More importantly, these reduction half reactions are mainly dependent on the thermodynamic reduction potentials required, instead of the number of electrons involved in the reactions. The reaction difficulty is decreased in the following order:

Table 1.4 The standard molar enthalpy ΔH^0_{298} and the Gibbs free energy ΔG^0_{298} for the reduction reactions of CO_2 with H_2O.

Reaction	ΔH^0_{298} ($kJ\,mol^{-1}$)	ΔG^0_{298} ($kJ\,mol^{-1}$)
$CO_2(g) + H_2O(l) \rightarrow HCOOH(l) + 1/2O_2(g)$	541	275
$CO_2(g) + H_2O(l) \rightarrow HCHO(l) + O_2(g)$	795.8	520
$CO_2(g) + H_2O(l) \rightarrow CH_3OH(l) + 3/2O_2(g)$	727.1	703
$CO_2(g) + H_2O(l) \rightarrow CH_4(g) + 2O_2(g)$	890.9	818

Table 1.5 The standard molar enthalpy ΔH^0_{298} and the Gibbs free energy ΔG^0_{298} of CO_2 hydrogenation reactions [351].

Reaction	ΔH^0_{298} (kJ mol^{-1})	ΔG^0_{298} (kJ mol^{-1})
$CO_2 + H_2 \rightarrow CO + H_2O(g)$	41.2	28.6
$CO_2 + H_2 \rightarrow HCOOH(l)$	−31.2	33.0
$CO_2 + 3H_2 \rightarrow CH_3OH + H_2O(l)$	−131.0	−9.0
$CO_2 + 4H_2 \rightarrow CH_4 + 2H_2O(g)$	−164.9	−113.5
$2CO_2 + 6H_2 \rightarrow C_2H_4 + 4H_2O(g)$	−127.91	−57.52
$3CO_2 + 9H_2 \rightarrow C_3H_6 + 6H_2O(g)$	−249.84	−125.69
$4CO_2 + 12H_2 \rightarrow C_4H_8 + 8H_2O(g)$	−360.44	−179.95

Source: Data from Chen et al. [351].

HCOOH (−0.61 eV), CO (−0.53 eV), HCHO (−0.48 eV), CH_3OH (−0.38 eV), and CH_4 (−0.24 eV). The Latimer–Frost diagram of CO_2 reduction by multiple electrons and protons in pH = 7 ionic solution (Figure 1.19) further confirms that the increase of the number of electrons could greatly decrease the reduction potential, making the CO_2 reduction much easier. On the other hand, a more negative CB bottom potential could achieve much stronger reduction ability for selective reduction of CO_2 into different products. At this point, semiconductors with selectivity for HCOOH formation must be used to achieve the reduction of CO_2 into other energy products with more positive reduction potentials such as CO, CH_4, CH_3OH, and HCHO. Therefore, g-C_3N_4, SiC, CdS, and ZnS with relatively negative CB bottom potentials can selectively reduce CO_2 to different products such as HCOOH, HCHO,

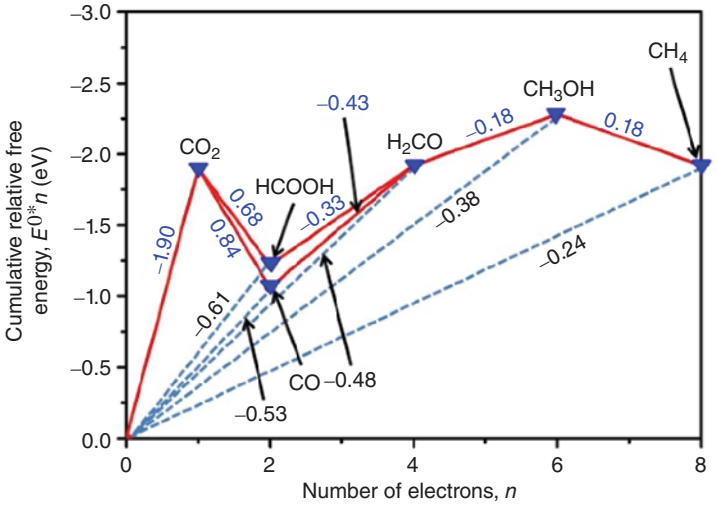

Figure 1.19 Latimer–Frost diagram for the multi-electron, multi-proton reduction of CO_2 in aqueous solution at pH 7. Source: Li et al. [352].

CH_3OH, or CH_4 [353–356]; whereas, rutile TiO_2 and $BiVO_4$ with relatively positive CB bottom potentials can reduce CO_2 and selectively produce CH_4, CH_3OH, or ethanol [357, 358]. Therefore, it is crucial to choose a semiconductor with suitable CB position in the selective reduction of CO_2 into different products.

Moreover, the dynamic factors, such as reaction conditions, the separation, and migration of photogenerated charge carriers, as well as the lifetime of electrons and holes, play key roles in highly efficient photoreduction of CO_2. Typically, the semiconductor photoreduction of CO_2 systems can be divided into two main categories: the aqueous suspension system (with dissolved CO_2 and carbonate) and the gas-phase reaction system (with water vapor and CO_2). The amount of H_2O in the aqueous suspension system is excessive, so it is impossible to adjust the ratio of H_2O/CO_2 by effective means for research. Therefore, more researchers choose the gas-phase system. Therefore, the gas–solid reaction model is used to analyze the influence of various factors on this kinetics of photocatalytic CO_2 reduction, as illustrated in Figure 1.20. It can be seen from the Figure 1.20 that in the process of photocatalytic reduction of CO_2, in addition to the excitation (process 1), charge transfer and separation (process 2), bulk recombination (process 3), and surface recombination (process 6) of photogenerated charge carriers, other important surface processes should also be considered, such as photocatalytic reduction of CO_2 (process 4) and water oxidation (process 5). In addition, we should pay attention to the undesired processes such as H_2 production on the surface of the photocatalyst (process 7) and

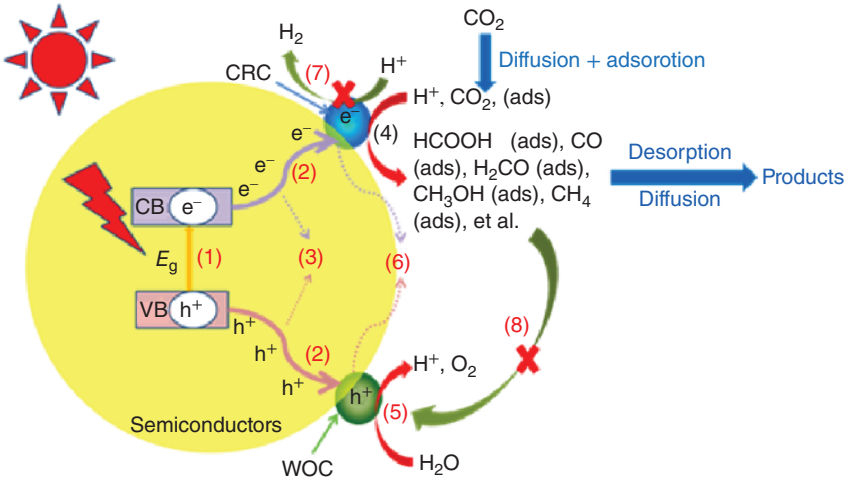

Figure 1.20 Processes involved in photocatalytic CO_2 reduction over a heterogeneous photocatalyst. CRC, CO_2 reduction cocatalysts; WOC, water oxidation cocatalysts. Step (1) the excitation of photogenerated electron–hole pairs; step (2) the separation of excited electrons and holes and their migration to the surface; step (3) the bulk charge recombination; step (4) the electrocatalytic reduction of CO_2 by photogenerated electrons trapped in the CRC or the surface active sites; step (5) the electrocatalytic oxidation of water by the photogenerated holes trapped in the WOC or the surface active sites; step (6) the surface charge recombination; step (7) the electrocatalytic H_2 evolution by trapped photogenerated electrons in the CRC or the surface active sites; and step (8) the electrocatalytic oxidation of reduction products over the WOC. Source: Li et al. [352].

re-oxidation of CO_2 reduction products (process 8). Therefore, from the viewpoint of system engineering, in order to build an efficient solar energy CO_2 conversion system, various possible factors, including the adsorption and activation of CO_2 by the photocatalytic materials, the efficiency of photogenerated electron–hole separation, the selection of cocatalysts, the promotion of target reactions (CO_2 reduction and water oxidation), and the inhibition of unexpected reactions (water reduction and re-oxidation of CO_2 reduction products), should be considered and optimized comprehensively.

In view of these key thermodynamic and kinetic factors affecting the efficiency of photocatalytic CO_2 reduction, Figure 1.21 systematically summarizes the corresponding design strategies of various high-efficiency photocatalytic CO_2 reduction photocatalysts [352]. These design strategies can be summarized into five aspects: (i) increasing the visible light absorption and excitation of photogenerated charge carriers, by means of elemental doping, introducing defects [359], building solid solutions, using the SPR effect [360], introducing photosensitizers, etc.; (ii) promoting carrier transfer and separation (mainly by building appropriate heterojunctions, such as Schott junction [355], type-II heterojunction [353, 354], direct Z-scheme system [80, 84], surface heterojunction [77, 361], and semiconductor/nanocarbon heterojunction [124, 125, 285, 362]); (iii) enhancing CO_2 adsorption and activation, such as increasing the surface area of the photocatalyst, introducing basic amino groups

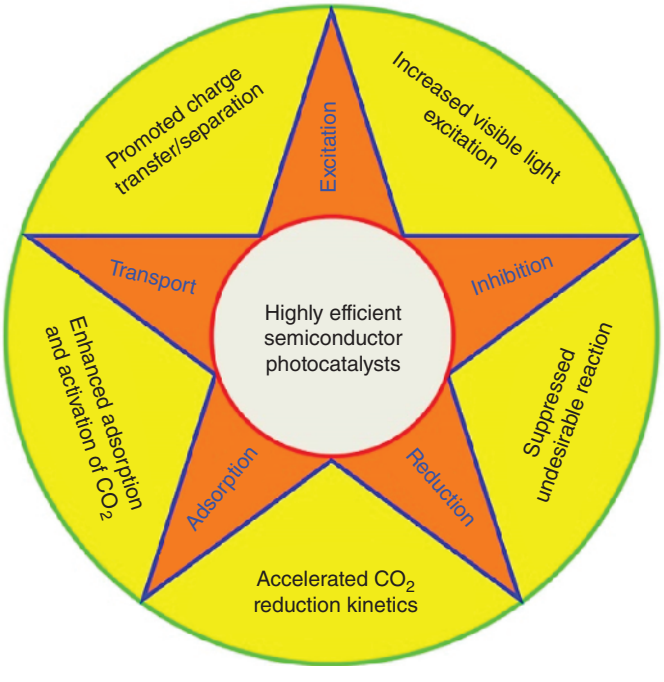

Figure 1.21 Factors influencing photocatalytic efficiency and corresponding design strategies for highly efficient photocatalysts used in the photocatalytic reduction of CO_2. Source: Li et al. [352].

[363, 364] or defect sites on the semiconductor surface; (iv) accelerating the reduction kinetics of CO_2 by loading various cocatalysts (such as Pt, AuCu alloy [365], RuO_x [366], and Ni@NiO [367]); and (v) inhibiting unexpected surface reactions, such as effectively inhibiting the H_2 generation reaction competing with carbon species for photogenerated electrons [368] and the re-oxidation reaction of the original product [369]. In the actual design of efficient CO_2 reduction photocatalysts, these modification strategies should be considered at the same time, so as to design the photocatalyst system with the best comprehensive performance.

In addition, the low selectivity and complex mechanism of photocatalytic reduction of CO_2 are also worthy of attention. So far, the use of photocatalytic reduction technology to synthesize organic compounds with CO_2 as raw material is still in the preliminary stage of research [134]. The key reason is that the conversion of CO_2 is not high and the selectivity of products is poor, due to the complex reaction mechanism. Considering the practical application of these compounds, it is highly desirable to control the selectivity of photocatalysts for a specific product and produce it with a purity as high as possible. However, the key factors affecting the selectivity of photocatalytic CO_2 reduction are still not well understood. So far, six typical strategies, including modulating surface morphological structures, tailoring surface chemical compositions, tuning the acidity–basicity of the supports, using the solvent effects, improving the interfacial properties, and loading suitable cocatalysts, have been explored to improve the product selectivity of the CO_2 photoreduction (as shown in Figure 1.22), which have been thoroughly discussed in a previous review [134].

1.5.1.3 Photocatalytic Degradation

In the past few decades, environmental pollution from discharge of toxic wastewater, solid waste, or flue gas has been regarded as a serious problem threating the sustainable development of human society. Semiconductor-based heterogeneous photocatalysis as an advanced oxidation process (AOP) has been extensively investigated for the pollution control and environmental remediation [370–375], due to its relatively easy operation and low costs. The photocatalytic degradation reactions could be generally classified into two types (Figure 1.23) [185]: (i) degradation of various organic pollutants (e.g. organic dyes, pharmaceuticals, antibiotics, pesticides, organic acids and aromatics, and recalcitrant polyfluorinated compounds [376, 377]) and toxic ions in aqueous solution and (ii) removal of gaseous pollutants (e.g. volatile organic compounds (VOCs), NO_x, ammonia, acetaldehyde, trichloroethylene, formaldehyde, and so on). Both types of photocatalytic reactions could be easily achieved in the laboratory by utilizing either photocatalyst powders or films immobilized on a support or substrate. However, industrial or pilot-scale applications of photocatalysis for environmental decontamination are still rare, due to unsatisfactory photocatalytic efficiency, selectivity, and stability of the currently developed photocatalysts.

According to the five design principles of semiconductor photocatalysts as shown in Figure 1.7, the potential practical photocatalysts for the degradation of pollutants could be evaluated. The stable, nontoxic, and inexpensive TiO_2 is the

Figure 1.22 Typical strategies for selective CO_2 photoreduction. Source: Li et al. [134].

most frequently and thoroughly investigated semiconductor in environmental applications, because it has the excellent photoactivity for both reduction of O_2 and oxidation of surface H_2O/hydroxyl group to generate reactive oxygen species (ROS) such as the superoxide radical anion ($^{\cdot}O_2^-$) and $^{\cdot}OH$ radicals, owing to its suitable energy band structure. Notably, ZnO exhibits similar activity for the formation of $^{\cdot}O_2^-$ and $^{\cdot}OH$ radicals. However, its low photostability induced by Zn^{2+} release significantly restricts its extensive applications; actually, ZnO nanoparticles can undergo substantial dissolution even in the absence of light. In the last decade, the environmentally benign g-C_3N_4 materials have been widely recognized as a promising family of next-generation semiconductors for visible light-driven photocatalysis, owing to the unique 2D structure, tunable electronic properties, and excellent chemical stability. However, it should be noted that the photogenerated holes in g-C_3N_4 cannot drive the oxidation of surface H_2O/OH groups to $^{\cdot}OH$ radicals, and any $^{\cdot}OH$ radicals generated by g-C_3N_4 are the result of further transformation of the $^{\cdot}O_2^-$ radicals. In addition, it should be pointed out that some visible light-driven semiconductors with more positive VB potentials, such as WO_3, $BiVO_4$, and Bi_2WO_6, have excellent abilities for the oxidation of surface H_2O/OH groups to $^{\cdot}OH$ radicals, suggesting their potential applications in environmental remediation. Particularly, the visible light-responsive Bi-based photocatalysts are appealing for the application of environmental photocatalysis. In contrast, the applications of CdS, $Zn_xCd_{1-x}S$, and Ag-based semiconductors in environmental remediation are not encouraged due to the toxicity of Cd, high cost of Ag, and their low stability. Accordingly, it is clear

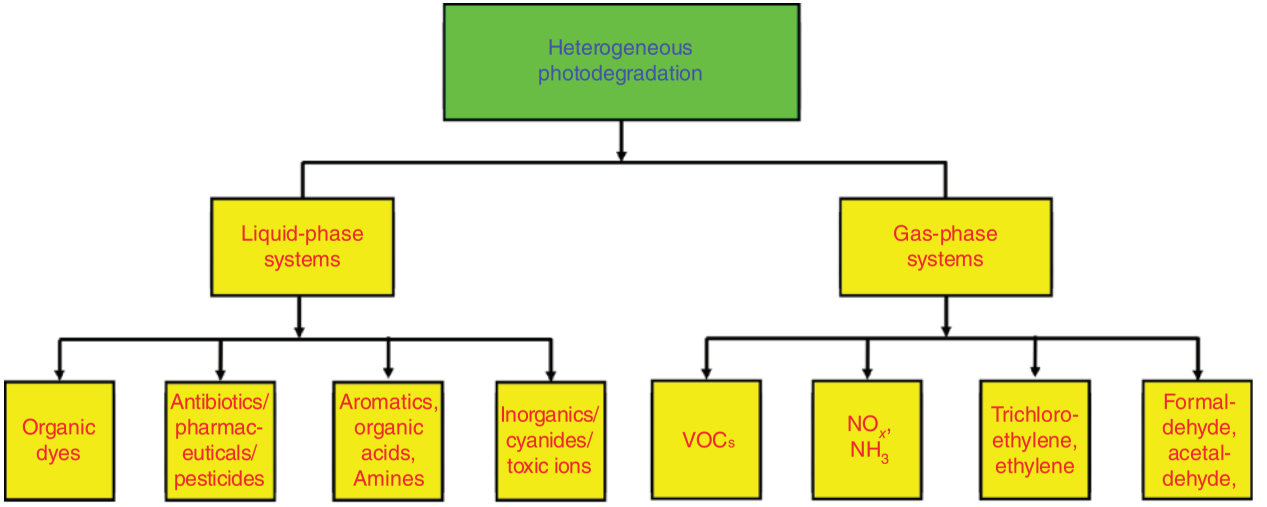

Figure 1.23 Heterogeneous photodegradation systems for various pollutants. Source: Li et al. [185].

that the thorough identification of ROS generation should be paid more attention in the investigations of photocatalytic environmental remediation.

In addition, due to the complex kinetics, bulk semiconductors commonly exhibit poor activity and stability to completely decompose the organic and inorganic contaminants. Many factors, such as light absorption, charge recombination dynamics, IFCT kinetics, surface structure and charge, and adsorption and photodegradation kinetics of photocatalysts, ROS generation, and O_2 reduction properties, play crucial roles in determining the overall photocatalytic degradation efficiency, all of which should be comprehensively considered for designing and optimizing environmental photocatalysts [370]. Accordingly, to effectively enhance the photocatalytic efficiency for durable degradation, a great number of semiconductor modification strategies have been exploited (Figure 1.24), such as creating semiconductor heterojunctions (type-II and multicomponent heterojunctions and homojunctions), constructing Schottky junctions or loading cocatalysts (e.g. coupling with metal nanoparticles and carbon nanomaterials), fabricating unique nanostructures (hollow one-dimensional (1D) nanorods/nanowires, 2D nanosheets, and three-dimensional (3D) hierarchical structures), loading suitable supports (e.g. activated carbon, Nafion, alumina, and silica), and designing the direct Z-scheme systems. Moreover, a combination of the different strategies seems to be very promising for heterogeneous photocatalytic degradation of pollutants, due to the simultaneously boosted light absorption, reactant adsorption, charge transport and separation, and surface catalysis.

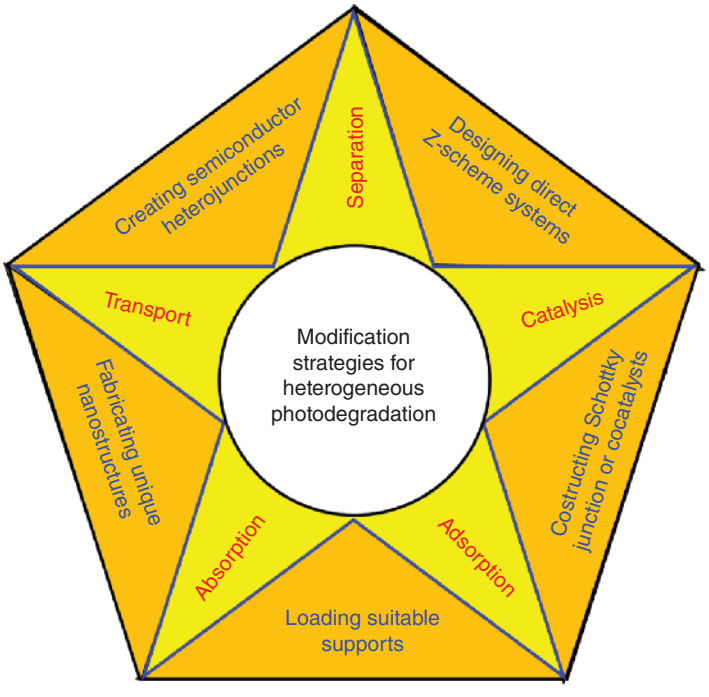

Figure 1.24 Semiconductor modification strategies for photocatalytic degradation. Source: Li et al. [185].

1.5.2 Evaluation of Solar Energy Photocatalysis

Evaluation of solar energy photocatalysis could be carried out according to the following three aspects: activity, photocatalytic mechanism, and semiconductor photocatalyst characterization. For the activity evaluation in different photocatalytic reactions, the stability and quantum efficiency should be examined in the practical applications. For the photocatalytic mechanism evaluation, the ROS species and reaction active sites should be carefully identified to elucidate the exact reaction mechanism. Additionally, the chemical composition, physical properties, and band

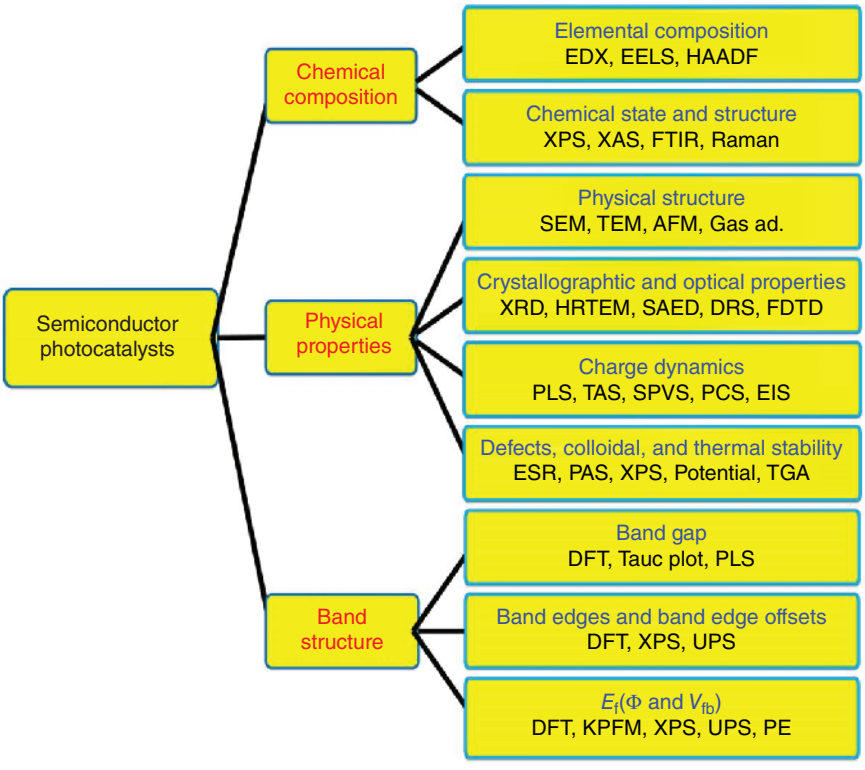

Figure 1.25 Characterization of some important properties of semiconductor photocatalysts. Source: Zhang et al. [378]. Abbreviations: E_f, Fermi level; f, work function; V_{fb}, flat-band potential; EDX, energy dispersive X-ray spectroscopy; EELS, electron energy-loss spectroscopy; HAADF, high-angle annular dark-field imaging; XPS, X-ray photoelectron spectroscopy; XAS, X-ray absorption spectroscopy; FTIR, Fourier transform infrared spectroscopy; SEM, scanning electron microscopy; TEM, transmission electron microscopy; AFM, atomic force microscopy; gas ad., gas adsorption–desorption analysis; XRD, X-ray diffraction; HRTEM, high-resolution transmission electron microscopy; SAED, selected area electron diffraction; DRS, diffuse reflectance spectroscopy; FDTD, finite-difference time-domain method; PLS, photoluminescence spectroscopy; TAS, transient absorption spectroscopy; SPVS, surface photovoltage spectroscopy; PCS, photocurrent spectroscopy; EIS, electrochemical impedance spectroscopy; ESR, electron spin resonance; PAS, positron annihilation spectroscopy; z potential, ζ potential; TGA, thermogravimetric analysis; DFT, density functional theory; UPS, ultraviolet photoelectron spectroscopy; KPFM, Kelvin probe force microscopy; PE, photoelectrochemical methods.

structure of semiconductor photocatalysts need to be properly analyzed by the different technologies listed in Figure 1.25 [378]. It should be noted that one or two technologies are applied to identify these properties. It is not necessary to use all these technologies to identify these properties in one time.

1.6 The Scope of This Book

So far, semiconductor photocatalysis technology has been widely used in many different fields, including photolysis of water for H_2 production, degradation of organic pollutants and heavy metal ions, or conversion of pollutants or CO_2 into solar fuel. As a new and effective way to deal with energy crisis and environmental problems, these areas have attracted growing attention, especially photocatalytic H_2 production and pollutant degradation. In recent years, the research on photocatalytic reduction of CO_2 and selective organic synthesis has gradually increased. Due to space limitation, this book focuses on the applications of different semiconductors in various photocatalytic research fields: photocatalytic decomposition of water for H_2 production, photocatalytic degradation of pollutants, and photocatalytic reduction of CO_2.

The book is roughly divided into six chapters. In Chapter 1, the fundamentals of solar energy photocatalysis are introduced. Chapter 2 focuses on various kinds of heterojunction systems for photocatalysis. In Chapter 3, the graphene-based photocatalysts are discussed. Chapter 4 focuses on the preparation of metal sulfide semiconductor photocatalysts and its application in the photocatalytic reactions. Chapter 5 and 6 focus on the preparation and applications of organic semiconductor photocatalysts and graphitic carbon nitride-based photocatalysts, respectively.

All in all, the selected content of this book is the hot research topics in semiconductor photocatalysts for different applications. The author hopes that this book will provide a professional, systematic, and up-to-date reference for researchers, who have been engaged in research in this field, as well as teachers and students. Solar energy photocatalysis is recognized as a very challenging research topic. We hope that this book can help you in the design, development, and improvement of new solar energy photocatalytic materials.

Acknowledgments

X. Li thanks National Natural Science Foundation of China (21975084, 51672089), Guangdong Provincial Applied Science and Technology Research and Development Program (2017B020238005), and the Ding Ying Talent Project of South China Agricultural University for their support.

References

1 Becquerel, A.E. (1839). Mémoire sur les effets électriques produits sous l'influence des rayons solaires. *Comptes Rendus* 9: 1839.

2 Brattain, W.H. and Garrett, C.G.B. (1955). Experiments on the interface between germanium and an electrolyte. *Bell Syst. Tech. J.* 34: 129–176.

3 Fujishima, A. and Honda, K. (1972). Electrochemical photolysis of water at a semiconductor electrode. *Nature* 238: 37–38.

4 Carey, J., Lawrence, J., and Tosine, H. (1976). Photodechlorination of PCB's in the presence of titanium dioxide in aqueous suspensions. *Bull. Environ. Contam. Toxicol.* 16: 697–701.

5 Frank, S.N. and Bard, A.J. (1977). Heterogeneous photocatalytic oxidation of cyanide ion in aqueous solutions at titanium dioxide powder. *J. Am. Chem. Soc.* 99: 303–304.

6 Schrauzer, G.N. and Guth, T.D. (1977). Photocatalytic reactions. 1. Photolysis of water and photoreduction of nitrogen on titanium dioxide. *J. Am. Chem. Soc.* 99: 7189–7193.

7 Kraeutler, B., Jaeger, C.D., and Bard, A.J. (1978). Direct observation of radical intermediates in the photo-Kolbe reaction – heterogeneous photocatalytic radical formation by electron spin resonance. *J. Am. Chem. Soc.* 100: 4903–4905.

8 Jaeger, C.D. and Bard, A.J. (1979). Spin trapping and electron spin resonance detection of radical intermediates in the photodecomposition of water at titanium dioxide particulate systems. *J. Phys. Chem.* 83: 3146–3152.

9 Kraeutler, B. and Bard, A.J. (1978). Heterogeneous photocatalytic preparation of supported catalysts. Photodeposition of platinum on titanium dioxide powder and other substrates. *J. Am. Chem. Soc.* 100: 4317–4318.

10 Kraeutler, B. and Bard, A.J. (1978). Heterogeneous photocatalytic synthesis of methane from acetic acid – new Kolbe reaction pathway. *J. Am. Chem. Soc.* 100: 2239–2240.

11 Bard, A.J. (1980). Photoelectrochemistry. *Science* 207: 139–144.

12 Bard, A.J. (1982). Design of semiconductor photoelectrochemical systems for solar energy conversion. *J. Phys. Chem.* 86: 172–177.

13 Halmann, M. (1978). Photoelectrochemical reduction of aqueous carbon dioxide on p-type gallium phosphide in liquid junction solar cells. *Nature* 275: 115–116.

14 Hemminger, J.C., Carr, R., and Somorjai, G.A. (1978). The photoassisted reaction of gaseous water and carbon dioxide adsorbed on the $SrTiO_3$ (111) crystal face to form methane. *Chem. Phys. Lett.* 57: 100–104.

15 Inoue, T., Fujishima, A., Konishi, S., and Honda, K. (1979). Photoelectrocatalytic reduction of carbon dioxide in aqueous suspensions of semiconductor powders. *Nature* 277: 637–638.

16 Kawai, T. and Sakata, T. (1980). Conversion of carbohydrate into hydrogen fuel by a photocatalytic process. *Nature* 286: 474–476.

17 Sato, S. and White, J.M. (1980). Photodecomposition of water over Pt/TiO_2 catalysts. *Chem. Phys. Lett.* 72: 83–86.

18 Wagner, F.T. and Somorjai, G.A. (1980). Photocatalytic hydrogen production from water on Pt-free $SrTiO_3$ in alkali hydroxide solutions. *Nature* 285: 559–560.

19 Wagner, F.T. and Somorjai, G.A. (1980). Photocatalytic and photoelectrochemical hydrogen production on strontium titanate single crystals. *J. Am. Chem. Soc.* 102: 5494–5502.

20 Bard, A.J. (1979). Photoelectrochemistry and heterogeneous photo-catalysis at semiconductors. *J. Photochem.* 10: 59–75.

21 Sato, S. and White, J.M. (1981). Photocatalytic water decomposition and water-gas shift reactions over NaOH-coated, platinized TiO_2. *J. Catal.* 69: 128–139.

22 Duonghong, D., Borgarello, E., and Graetzel, M. (1981). Dynamics of light-induced water cleavage in colloidal systems. *J. Am. Chem. Soc.* 103: 4685–4690.

23 Grätzel, M. (1981). Artificial photosynthesis: water cleavage into hydrogen and oxygen by visible light. *Acc. Chem. Res.* 14: 376–384.

24 Domen, K., Naito, S., Onishi, T. et al. (1982). Study of the photocatalytic decomposition of water vapor over a nickel(II) oxide-strontium titanate ($SrTiO_3$) catalyst. *J. Phys. Chem.* 86: 3657–3661.

25 Serpone, N., Borgarello, E., and Grätzel, M. (1984). Visible light induced generation of hydrogen from H_2S in mixed semiconductor dispersions, improved efficiency through inter-particle electron transfer. *J. Chem. Soc., Chem. Commun.*: 342–344.

26 Kakuta, N., Park, K.H., Finlayson, M.F. et al. (1985). Photoassisted hydrogen production using visible light and coprecipitated zinc sulfide.cntdot.cadmium sulfide without a noble metal. *J. Phys. Chem.* 89: 732–734.

27 Domen, K., Kudo, A., and Onishi, T. (1986). Mechanism of photocatalytic decomposition of water into H_2 and O_2 over $NiO\text{-}SrTiO_3$. *J. Catal.* 102: 92–98.

28 Domen, K., Kudo, A., Onishi, T. et al. (1986). Photocatalytic decomposition of water into hydrogen and oxygen over nickel(II) oxide-strontium titanate ($SrTiO_3$) powder. 1. Structure of the catalysts. *J. Phys. Chem.* 90: 292–295.

29 Anpo, M., Shima, T., Kodama, S., and Kubokawa, Y. (1987). Photocatalytic hydrogenation of propyne with water on small-particle titania: size quantization effects and reaction intermediates. *J. Phys. Chem.* 91: 4305–4310.

30 O'Regan, B. and Gratzel, M. (1991). A low-cost, high-efficiency solar cell based on dye-sensitized colloidal TiO_2 films. *Nature* 353: 737–740.

31 Choi, W., Termin, A., and Hoffmann, M.R. (1994). The role of metal ion dopants in quantum-sized TiO_2: correlation between photoreactivity and charge carrier recombination dynamics. *J. Phys. Chem.* 98: 13669–13679.

32 Wang, R., Hashimoto, K., Fujishima, A. et al. (1997). Light-induced amphiphilic surfaces. *Nature* 388: 431–432.

33 Kudo, A., Ueda, K., Kato, H., and Mikami, I. (1998). Photocatalytic O_2 evolution under visible light irradiation on $BiVO_4$ in aqueous $AgNO_3$ solution. *Catal. Lett.* 53: 229–230.

34 Kudo, A., Omori, K., and Kato, H. (1999). A novel aqueous process for preparation of crystal form-controlled and highly crystalline $BiVO_4$ powder from layered vanadates at room temperature and its photocatalytic and photophysical properties. *J. Am. Chem. Soc.* 121: 11459–11467.

35 Zou, Z., Ye, J., Sayama, K., and Arakawa, H. (2001). Direct splitting of water under visible light irradiation with an oxide semiconductor photocatalyst. *Nature* 414: 625–627.

36 Grätzel, M. (2001). Photoelectrochemical cells. *Nature* 414: 338–344.

37 Asahi, R., Morikawa, T., Ohwaki, T. et al. (2001). Visible-light photocatalysis in nitrogen-doped titanium oxides. *Science* 293: 269–271.

38 Abe, R., Sayama, K., Domen, K., and Arakawa, H. (2001). A new type of water splitting system composed of two different TiO_2 photocatalysts (anatase, rutile) and a IO_3^-/I^- shuttle redox mediator. *Chem. Phys. Lett.* 344: 339–344.

39 Khan, S.U.M., Al-Shahry, M., and Ingler, W.B. (2002). Efficient photochemical water splitting by a chemically modified n-TiO_2. *Science* 297: 2243–2245.

40 Yu, J.C., Yu, J.G., Ho, W.K. et al. (2002). Effects of F^- doping on the photocatalytic activity and microstructures of nanocrystalline TiO_2 powders. *Chem. Mater.* 14: 3808–3816.

41 Hitoki, G., Ishikawa, A., Takata, T. et al. (2002). Ta_3N_5 as a novel visible light-driven photocatalyst (λ<600 nm). *Chem. Lett.* 31: 736–737.

42 Hitoki, G., Takata, T., Kondo, J.N. et al. (2002). An oxynitride, TaON, as an efficient water oxidation photocatalyst under visible light irradiation ($\lambda \leq$500 nm). *Chem. Commun.* 38: 1698–1699.

43 Kudo, A., Tsuji, I., and Kato, H. (2002). $AgInZn_7S_9$ solid solution photocatalyst for H_2 evolution from aqueous solutions under visible light irradiation. *Chem. Commun.* 38: 1958–1959.

44 Zhang, L.Z. and Yu, J.C. (2003). A sonochemical approach to hierarchical porous titania spheres with enhanced photocatalytic activity. *Chem. Commun.* 39: 2078–2079.

45 Wang, X.C., Yu, J.C., Ho, C.M. et al. (2005). Photocatalytic activity of a hierarchically macro/mesoporous titania. *Langmuir* 21: 2552–2559.

46 Kato, H., Asakura, K., and Kudo, A. (2003). Highly efficient water splitting into H_2 and O_2 over lanthanum-doped $NaTaO_3$ photocatalysts with high crystallinity and surface nanostructure. *J. Am. Chem. Soc.* 125: 3082–3089.

47 Tsuji, I., Kato, H., Kobayashi, H., and Kudo, A. (2004). Photocatalytic H_2 evolution reaction from aqueous solutions over band structure-controlled $(AgIn)_xZn_{2(1-x)}S_2$ solid solution photocatalysts with visible-light response and their surface nanostructures. *J. Am. Chem. Soc.* 126: 13406–13413.

48 Maeda, K., Takata, T., Hara, M. et al. (2005). GaN:ZnO solid solution as a photocatalyst for visible-light-driven overall water splitting. *J. Am. Chem. Soc.* 127: 8286–8287.

49 Maeda, K., Teramura, K., Takata, T. et al. (2005). Overall water splitting on $(Ga_{1-x}Zn_x)(N_{1-x}O_x)$ solid solution photocatalyst: relationship between physical properties and photocatalytic activity. *J. Phys. Chem. B* 109: 20504–20510.

50 Maeda, K., Teramura, K., Lu, D.L. et al. (2006). Photocatalyst releasing hydrogen from water – enhancing catalytic performance holds promise for hydrogen production by water splitting in sunlight. *Nature* 440: 295–295.

51 Tada, H., Mitsui, T., Kiyonaga, T. et al. (2006). All-solid-state Z-scheme in CdS-Au-TiO_2 three-component nanojunction system. *Nat. Mater.* 5: 782–786.

52 Yu, J., Guo, H., Davis, S.A., and Mann, S. (2006). Fabrication of hollow inorganic microspheres by chemically induced self-transformation. *Adv. Funct. Mater.* 16: 2035–2041.

53 Yu, J., Liu, S., and Yu, H. (2007). Microstructures and photoactivity of mesoporous anatase hollow microspheres fabricated by fluoride-mediated self-transformation. *J. Catal.* 249: 59–66.

54 Zhang, X., Ai, Z., Jia, F., and Zhang, L. (2008). Generalized one-pot synthesis, characterization, and photocatalytic activity of hierarchical BiOX (X = Cl, Br, I) nanoplate microspheres. *J. Phys. Chem. C* 112: 747–753.

55 Williams, G., Seger, B., and Kamat, P.V. (2008). TiO_2-graphene nanocomposites. UV-assisted photocatalytic reduction of graphene oxide. *ACS Nano* 2: 1487–1491.

56 Tian, Y. and Tatsuma, T. (2005). Mechanisms and applications of plasmon-induced charge separation at TiO_2 films loaded with gold nanoparticles. *J. Am. Chem. Soc.* 127: 7632–7637.

57 Yang, H.G., Sun, C.H., Qiao, S.Z. et al. (2008). Anatase TiO_2 single crystals with a large percentage of reactive facets. *Nature* 453: 638–641.

58 Zong, X., Yan, H., Wu, G. et al. (2008). Enhancement of photocatalytic H_2 evolution on CdS by loading MoS_2 as cocatalyst under visible light irradiation. *J. Am. Chem. Soc.* 130: 7176–7177.

59 Wang, X., Maeda, K., Thomas, A. et al. (2009). A metal-free polymeric photocatalyst for hydrogen production from water under visible light. *Nat. Mater.* 8: 76–80.

60 Yan, H., Yang, J., Ma, G. et al. (2009). Visible-light-driven hydrogen production with extremely high quantum efficiency on Pt–PdS/CdS photocatalyst. *J. Catal.* 266: 165–168.

61 Wang, X.W., Liu, G., Chen, Z.G. et al. (2009). Enhanced photocatalytic hydrogen evolution by prolonging the lifetime of carriers in ZnO/CdS heterostructures. *Chem. Commun.* 45: 3452–3454.

62 Maeda, K., Higashi, M., Lu, D.L. et al. (2010). Efficient nonsacrificial water splitting through two-step photoexcitation by visible light using a modified oxynitride as a hydrogen evolution photocatalyst. *J. Am. Chem. Soc.* 132: 5858–5868.

63 Zhang, W., Wang, Y., Wang, Z. et al. (2010). Highly efficient and noble metal-free NiS/CdS photocatalysts for H_2 evolution from lactic acid sacrificial solution under visible light. *Chem. Commun.* 46: 7631–7633.

64 Varghese, O.K., Paulose, M., LaTempa, T.J., and Grimes, C.A. (2009). High-rate solar photocatalytic conversion of CO_2 and water vapor to hydrocarbon fuels. *Nano Lett.* 9: 731–737.

65 Yi, Z.G., Ye, J.H., Kikugawa, N. et al. (2010). An orthophosphate semiconductor with photooxidation properties under visible-light irradiation. *Nat. Mater.* 9: 559–564.

66 Liu, S., Yu, J., and Jaroniec, M. (2010). Tunable photocatalytic selectivity of hollow TiO_2 microspheres composed of anatase polyhedra with exposed {001} facets. *J. Am. Chem. Soc.* 132: 11914–11916.

67 Chen, X.B., Liu, L., Yu, P.Y., and Mao, S.S. (2011). Increasing solar absorption for photocatalysis with black hydrogenated titanium dioxide nanocrystals. *Science* 331: 746–750.

68 Li, Q., Guo, B., Yu, J. et al. (2011). Highly efficient visible-light-driven photocatalytic hydrogen production of CdS-cluster-decorated graphene nanosheets. *J. Am. Chem. Soc.* 133: 10878–10884.

69 Iwase, A., Ng, Y.H., Ishiguro, Y. et al. (2011). Reduced graphene oxide as a solid-state electron mediator in Z-scheme photocatalytic water splitting under visible light. *J. Am. Chem. Soc.* 133: 11054–11057.

70 Yu, J. and Ran, J. (2011). Facile preparation and enhanced photocatalytic H_2-production activity of $Cu(OH)_2$ cluster modified TiO_2. *Energy Environ. Sci.* 4: 1364–1371.

71 Yu, J., Hai, Y., and Cheng, B. (2011). Enhanced photocatalytic H_2-production activity of TiO_2 by $Ni(OH)_2$ cluster modification. *J. Phys. Chem. C* 115: 4953–4958.

72 Zhang, J., Yu, J., Zhang, Y. et al. (2011). Visible light photocatalytic H_2-production activity of CuS/ZnS porous nanosheets based on photoinduced interfacial charge transfer. *Nano Lett.* 11: 4774–4779.

73 Wang, W.N., An, W.J., Ramalingam, B. et al. (2012). Size and structure matter: enhanced CO_2 photoreduction efficiency by size-resolved ultrafine Pt nanoparticles on TiO_2 single crystals. *J. Am. Chem. Soc.* 134: 11276–11281.

74 Xiang, Q., Yu, J., and Jaroniec, M. (2012). Synergetic effect of MoS_2 and graphene as cocatalysts for enhanced photocatalytic H_2 production activity of TiO_2 nanoparticles. *J. Am. Chem. Soc.* 134: 6575–6578.

75 Zhang, J., Yu, J., Jaroniec, M., and Gong, J.R. (2012). Noble metal-free reduced graphene oxide-$Zn_xCd_{1-x}S$ nanocomposite with enhanced solar photocatalytic H_2-production performance. *Nano Lett.* 12: 4584–4589.

76 Yu, J., Wang, S., Low, J., and Xiao, W. (2013). Enhanced photocatalytic performance of direct Z-scheme g-C_3N_4-TiO_2 photocatalysts for the decomposition of formaldehyde in air. *Phys. Chem. Chem. Phys.* 15: 16883–16890.

77 Yu, J., Low, J., Xiao, W. et al. (2014). Enhanced photocatalytic CO_2-reduction activity of anatase TiO_2 by coexposed {001} and {101} facets. *J. Am. Chem. Soc.* 136: 8839–8842.

78 Zhang, J., Qi, L., Ran, J. et al. (2014). Ternary NiS/$Zn_xCd_{1-x}S$/reduced graphene oxide nanocomposites for enhanced solar photocatalytic H_2-production activity. *Adv. Energy Mater.* 4: 1301925.

79 Liu, J., Liu, Y., Liu, N. et al. (2015). Metal-free efficient photocatalyst for stable visible water splitting via a two-electron pathway. *Science* 347: 970–974.

80 Jin, J., Yu, J., Guo, D. et al. (2015). A hierarchical Z-scheme CdS-WO_3 photocatalyst with enhanced CO_2 reduction activity. *Small* 11: 5262–5271.

81 Chen, J., Wu, X.J., Yin, L. et al. (2015). One-pot synthesis of CdS nanocrystals hybridized with single-layer transition-metal dichalcogenide nanosheets for efficient photocatalytic hydrogen evolution. *Angew. Chem. Int. Ed.* 54: 1210–1214.

82 Ghosh, S., Kouame, N.A., Ramos, L. et al. (2015). Conducting polymer nanostructures for photocatalysis under visible light. *Nat. Mater.* 14: 505–511.

83 Ong, W.J., Tan, L.L., Chai, S.P., and Yong, S.T. (2015). Graphene oxide as a structure-directing agent for the two-dimensional interface engineering of sandwich-like graphene-g-C_3N_4 hybrid nanostructures with enhanced visible-light photoreduction of CO_2 to methane. *Chem. Commun.* 51: 858–861.

84 Yu, W., Xu, D., and Peng, T. (2015). Enhanced photocatalytic activity of g-C_3N_4 for selective CO_2 reduction to CH_3OH via facile coupling of ZnO: a direct Z-scheme mechanism. *J. Mater. Chem. A* 3: 19936–19947.

85 Low, J., Cheng, B., Yu, J., and Jaroniec, M. (2016). Carbon-based two-dimensional layered materials for photocatalytic CO_2 reduction to solar fuels. *Energy Storage Mater.* 3: 24–35.

86 Ma, T.Y., Cao, J.L., Jaroniec, M., and Qiao, S.Z. (2016). Interacting carbon nitride and titanium carbide nanosheets for high-performance oxygen evolution. *Angew. Chem. Int. Ed.* 55: 1138–1142.

87 Wang, Q., Hisatomi, T., Jia, Q. et al. (2016). Scalable water splitting on particulate photocatalyst sheets with a solar-to-hydrogen energy conversion efficiency exceeding 1%. *Nat. Mater.* 15: 611–615.

88 Zhang, B., Zheng, X.L., Voznyy, O. et al. (2016). Homogeneously dispersed multimetal oxygen-evolving catalysts. *Science* 352: 333–337.

89 Huang, Z.F., Song, J., Li, K. et al. (2016). Hollow cobalt-based bimetallic sulfide polyhedra for efficient all-pH-value electrochemical and photocatalytic hydrogen evolution. *J. Am. Chem. Soc.* 138: 1359–1365.

90 Zhou, X., Liu, R., Sun, K. et al. (2016). Solar-driven reduction of 1 atm of CO_2 to formate at 10% energy-conversion efficiency by use of a TiO_2-protected III-V tandem photoanode in conjunction with a bipolar membrane and a Pd/C cathode. *Acs Energy Lett.* 1: 764–770.

91 Fu, J., Zhu, B., Jiang, C. et al. (2017). Hierarchical porous O-doped g-C_3N_4 with enhanced photocatalytic CO_2 reduction activity. *Small* 13: 1603938.

92 Zhu, M., Cai, X., Fujitsuka, M. et al. (2017). Au/$La_2Ti_2O_7$ nanostructures sensitized with black phosphorus for plasmon-enhanced photocatalytic hydrogen production in visible and near-infrared light. *Angew. Chem. Int. Ed.* 56: 2064–2068.

93 Zhu, X., Zhang, T., Sun, Z. et al. (2017). Black phosphorus revisited: a missing metal-free elemental photocatalyst for visible light hydrogen evolution. *Adv. Mater.* 29: 1605776.

94 Ran, J., Gao, G., Li, F.T. et al. (2017). Ti_3C_2 MXene co-catalyst on metal sulfide photo-absorbers for enhanced visible-light photocatalytic hydrogen production. *Nat. Commun.* 8: 13907.

95 Chai, Z., Zeng, T.T., Li, Q. et al. (2016). Efficient visible light-driven splitting of alcohols into hydrogen and corresponding carbonyl compounds over a Ni-modified CdS photocatalyst. *J. Am. Chem. Soc.* 138: 10128–10131.

96 Che, W., Cheng, W., Yao, T. et al. (2017). Fast photoelectron transfer in (Cring)–C_3N_4 plane heterostructural nanosheets for overall water splitting. *J. Am. Chem. Soc.* 139: 3021–3026.

97 Zhang, Z.Y., Huang, J.D., Fang, Y.R. et al. (2017). A nonmetal plasmonic Z-scheme photocatalyst with UV- to NIR-driven photocatalytic protons reduction. *Adv. Mater.* 29: 1606688.

98 Hirakawa, H., Hashimoto, M., Shiraishi, Y., and Hirai, T. (2017). Photocatalytic conversion of nitrogen to ammonia with water on surface oxygen vacancies of titanium dioxide. *J. Am. Chem. Soc.* 139: 10929–10936.

99 Jiao, X.C., Chen, Z.W., Li, X.D. et al. (2017). Defect-mediated electron-hole separation in one-unit-cell $ZnIn_2S_4$ layers for boosted solar-driven CO_2 reduction. *J. Am. Chem. Soc.* 139: 7586–7594.

100 Xu, Y.F., Yang, M.Z., Chen, B.X. et al. (2017). A $CsPbBr_3$ perovskite quantum dot/graphene oxide composite for photocatalytic CO_2 reduction. *J. Am. Chem. Soc.* 139: 5660–5663.

101 Park, S., Chang, W.J., Lee, C.W. et al. (2017). Photocatalytic hydrogen generation from hydriodic acid using methylammonium lead iodide in dynamic equilibrium with aqueous solution. *Nat. Energy* 2: 16185.

102 Zhu, M.S., Kim, S., Mao, L. et al. (2017). Metal-free photocatalyst for H_2 evolution in visible to near-infrared region: black phosphorus/graphitic carbon nitride. *J. Am. Chem. Soc.* 139: 13234–13242.

103 Wen, J.Q., Xie, J., Zhang, H.D. et al. (2017). Constructing multifunctional metallic Ni interface layers in the g-C_3N_4 nanosheets/amorphous NiS heterojunctions for efficient photocatalytic H_2 generation. *ACS Appl. Mater. Interfaces* 9: 14031–14042.

104 Qi, Y., Zhao, Y., Gao, Y.Y. et al. (2018). Redox-based visible-light-driven Z-scheme overall water splitting with apparent quantum efficiency exceeding 10%. *Joule* 2: 2393–2402.

105 Pachfule, P., Acharjya, A., Roeser, J. et al. (2018). Diacetylene functionalized covalent organic framework (COF) for photocatalytic hydrogen generation. *J. Am. Chem. Soc.* 140: 1423–1427.

106 Chen, R.T., Pang, S., An, H.Y. et al. (2018). Charge separation via asymmetric illumination in photocatalytic Cu_2O particles. *Nat. Energy* 3: 655–663.

107 Ma, S., Deng, Y.P., Xie, J. et al. (2018). Noble-metal-free Ni_3C cocatalysts decorated CdS nanosheets for high efficiency visible-light-driven photocatalytic H_2 evolution. *Appl. Catal., B* 227: 218–228.

108 Shi, R., Ye, H.F., Liang, F. et al. (2018). Interstitial P-doped CdS with long-lived photogenerated electrons for photocatalytic water splitting without sacrificial agents. *Adv. Mater.* 30: 1705941.

109 Xu, F.Y., Meng, K., Zhu, B.C. et al. (2019). A new photocatalytic CO_2 reduction cocatalyst. *Adv. Funct. Mater.* 29: 1904256.

110 Fu, J.W., Xu, Q.L., Low, J.X. et al. (2019). Ultrathin 2D/2D WO_3/g-C_3N_4 step-scheme H_2-production photocatalyst. *Appl. Catal., B* 243: 556–565.

111 Low, J.X., Dai, B.Z., Tong, T. et al. (2019). In situ irradiated X-ray photoelectron spectroscopy investigation on a direct Z-scheme TiO_2/CdS composite film photocatalyst. *Adv. Mater.* 31: 5.

112 Kumar, P., Vahidzadeh, E., Thakur, W.K. et al. (2019). C_3N_5: A low bandgap semiconductor containing an azo-linked carbon nitride framework for photocatalytic, photovoltaic and adsorbent applications. *J. Am. Chem. Soc.* 141: 5415–5436.

113 Li, X.D., Sun, Y.F., Xu, J.Q. et al. (2019). Selective visible-light-driven photocatalytic CO_2 reduction to CH_4 mediated by atomically thin $CuIn_5S_8$ layers. *Nat. Energy* 4: 690–699.

114 Lee, B.H., Park, S., Kim, M. et al. (2019). Reversible and cooperative photoactivation of single-atom Cu/TiO_2 photocatalysts. *Nat. Mater.* 18: 620–626.

115 Shiraishi, Y., Takii, T., Hagi, T. et al. (2019). Resorcinol-formaldehyde resins as metal-free semiconductor photocatalysts for solar-to-hydrogen peroxide energy conversion. *Nat. Mater.* 18: 985–993.

116 Wang, Q., Nakabayashi, M., Hisatomi, T. et al. (2019). Oxysulfide photocatalyst for visible-light-driven overall water splitting. *Nat. Mater.* 18: 827–832.

117 Takata, T., Jiang, J., Sakata, Y. et al. (2020). Photocatalytic water splitting with a quantum efficiency of almost unity. *Nature* 581: 411–414.

118 Ni, M., Leung, M.K.H., Leung, D.Y.C., and Sumathy, K. (2007). A review and recent developments in photocatalytic water-splitting using TiO_2 for hydrogen production. *Renewable Sustainable Energy Rev.* 11: 401–425.

119 Wang, P., Huang, B., Qin, X. et al. (2008). Ag@AgCl: a highly efficient and stable photocatalyst active under visible light. *Angew. Chem. Int. Ed.* 47: 7931–7933.

120 Cao, S., Low, J., Yu, J., and Jaroniec, M. (2015). Polymeric photocatalysts based on graphitic carbon nitride. *Adv. Mater.* 27: 2150–2176.

121 Wen, J., Xie, J., Chen, X., and Li, X. (2017). A review on g-C_3N_4-based photocatalysts. *Appl. Surf. Sci.* 391: 72–123.

122 Ong, W.J., Tan, L.L., Ng, Y.H. et al. (2016). Graphitic carbon nitride (g-C_3N_4)-based photocatalysts for artificial photosynthesis and environmental remediation: are we a step closer to achieving sustainability? *Chem. Rev.* 116: 7159–7329.

123 Cao, S. and Yu, J. (2014). g-C_3N_4-based photocatalysts for hydrogen generation. *J. Phys. Chem. Lett.* 5: 2101–2107.

124 Xiang, Q., Cheng, B., and Yu, J. (2015). Graphene-based photocatalysts for solar-fuel generation. *Angew. Chem. Int. Ed.* 54: 11350–11366.

125 Yu, J., Jin, J., Cheng, B., and Jaroniec, M. (2014). A noble metal-free reduced graphene oxide-CdS nanorod composite for the enhanced visible-light photocatalytic reduction of CO_2 to solar fuel. *J. Mater. Chem. A* 2: 3407–3416.

126 Li, Q., Li, X., Wageh, S. et al. (2015). Graphene nanocomposite photocatalysts. *Adv. Energy Mater.* 5: 1500010.

127 Li, X., Yu, J., Wageh, S. et al. (2016). Graphene in photocatalysis: a review. *Small* 12: 6640–6696.

128 Zhou, P., Yu, J., and Jaroniec, M. (2014). All-solid-state Z-scheme photocatalytic systems. *Adv. Mater.* 26: 4920–4935.

129 Low, J., Jiang, C., Cheng, B. et al. (2017). A review of direct Z-scheme photocatalysts. *Small Methods* 1: 1700080.

130 He, K., Xie, J., Luo, X. et al. (2017). Enhanced visible light photocatalytic H_2 production over Z-scheme g-C_3N_4 nansheets/WO_3 nanorods nanocomposites loaded with $Ni(OH)_x$ cocatalysts. *Chin. J. Catal.* 38: 240–252.

131 Iqbal, S., Pan, Z., and Zhou, K. (2017). Enhanced photocatalytic hydrogen evolution from in situ formation of few-layered MoS_2/CdS nanosheet-based van der Waals heterostructures. *Nanoscale* 9: 6638–6642.

132 Xiang, Q., Yu, J., and Jaroniec, M. (2011). Preparation and enhanced visible-light photocatalytic H_2-production activity of graphene/C_3N_4 composites. *J. Phys. Chem. C* 115: 7355–7363.

133 Yuan, J., Wen, J., Zhong, Y. et al. (2015). Enhanced photocatalytic H_2 evolution over noble-metal-free NiS cocatalyst modified CdS nanorods/g-C_3N_4 heterojunctions. *J. Mater. Chem. A* 3: 18244–18255.

134 Li, X., Yu, J.G., Jaroniec, M., and Chen, X.B. (2019). Cocatalysts for selective photoreduction of CO_2 into solar fuels. *Chem. Rev.* 119: 3962–4179.

135 Wen, J., Li, X., Liu, W. et al. (2015). Photocatalysis fundamentals and surface modification of TiO_2 nanomaterials. *Chin. J. Catal.* 36: 2049–2070.

136 Kumar, S.G. and Rao, K.S.R.K. (2015). Tungsten-based nanomaterials (WO_3 & Bi_2WO_6): modifications related to charge carrier transfer mechanisms and photocatalytic applications. *Appl. Surf. Sci.* 355: 939–958.

137 Kuang, P.Y., Zheng, P.X., Liu, Z.Q. et al. (2016). Embedding Au quantum dots in rimous cadmium sulfide nanospheres for enhanced photocatalytic hydrogen evolution. *Small* 12: 6735–6744.

138 He, R.a., Cao, S., Zhou, P., and Yu, J. (2014). Recent advances in visible light Bi-based photocatalysts. *Chin. J. Catal.* 35: 989–1007.

139 Zhang, X.H., Peng, T.Y., and Song, S.S. (2016). Recent advances in dye-sensitized semiconductor systems for photocatalytic hydrogen production. *J. Mater. Chem. A* 4: 2365–2402.

140 Morris, A.J., Meyer, G.J., and Fujita, E. (2009). Molecular approaches to the photocatalytic reduction of carbon dioxide for solar fuels. *Acc. Chem. Res.* 42: 1983–1994.

141 Esswein, A.J. and Nocera, D.G. (2007). Hydrogen production by molecular photocatalysis. *Chem. Rev.* 107: 4022–4047.

142 Takeda, H. and Ishitani, O. (2010). Development of efficient photocatalytic systems for CO_2 reduction using mononuclear and multinuclear metal complexes based on mechanistic studies. *Coord. Chem. Rev.* 254: 346–354.

143 Windle, C.D. and Perutz, R.N. (2012). Advances in molecular photocatalytic and electrocatalytic CO_2 reduction. *Coord. Chem. Rev.* 256: 2562–2570.

144 Sprick, R.S., Bonillo, B., Clowes, R. et al. (2016). Visible-light-driven hydrogen evolution using planarized conjugated polymer photocatalysts. *Angew. Chem. Int. Ed.* 55: 1824–1828.

145 Muktha, B., Madras, G., Row, T.N.G. et al. (2007). Conjugated polymers for photocatalysis. *J. Phys. Chem. B* 111: 7994–7998.

146 Li, L., Cai, Z., Wu, Q. et al. (2016). Rational design of porous conjugated polymers and roles of residual palladium for photocatalytic hydrogen production. *J. Am. Chem. Soc.* 138: 7681–7686.

147 Zhou, Q. and Shi, G. (2016). Conducting polymer-based catalysts. *J. Am. Chem. Soc.* 138: 2868–2876.

148 Yeh, T.F., Syu, J.M., Cheng, C. et al. (2010). Graphite oxide as a photocatalyst for hydrogen production from water. *Adv. Funct. Mater.* 20: 2255–2262.

149 Chen, X. and Mao, S.S. (2007). Titanium dioxide nanomaterials: synthesis, properties, modifications, and applications. *Chem. Rev.* 107: 2891–2959.

150 Rehman, S., Ullah, R., Butt, A.M., and Gohar, N.D. (2009). Strategies of making TiO_2 and ZnO visible light active. *J. Hazard. Mater.* 170: 560–569.

151 Li, X., Yu, J., Low, J. et al. (2015). Engineering heterogeneous semiconductors for solar water splitting. *J. Mater. Chem. A* 3: 2485–2534.

152 Chen, X., Shen, S., Guo, L., and Mao, S.S. (2010). Semiconductor-based photocatalytic hydrogen generation. *Chem. Rev.* 110: 6503–6570.

153 Dong, F., Xiong, T., Sun, Y. et al. (2014). A semimetal bismuth element as a direct plasmonic photocatalyst. *Chem. Commun.* 50: 10386–10389.

154 Zhang, Q., Zhou, Y., Wang, F. et al. (2014). From semiconductors to semimetals: bismuth as a photocatalyst for NO oxidation in air. *J. Mater. Chem. A* 2: 11065–11072.

155 Zhao, Z., Zhang, W., Sun, Y. et al. (2016). Bi cocatalyst/Bi_2MoO_6 microspheres nanohybrid with SPR-promoted visible-light photocatalysis. *J. Phys. Chem. C* 120: 11889–11898.

156 Sun, Y., Zhao, Z., Dong, F., and Zhang, W. (2015). Mechanism of visible light photocatalytic NO_x oxidation with plasmonic Bi cocatalyst-enhanced $(BiO)_2CO_3$ hierarchical microspheres. *Phys. Chem. Chem. Phys.* 17: 10383–10390.

157 Dong, F., Zhao, Z., Sun, Y. et al. (2015). An advanced semimetal-organic Bi spheres-g-C_3N_4 nanohybrid with SPR-enhanced visible-light photocatalytic performance for NO purification. *Environ. Sci. Technol.* 49: 12432–12440.

158 Dong, F., Li, Q., Sun, Y., and Ho, W.K. (2014). Noble metal-like behavior of plasmonic Bi particles as a cocatalyst deposited on $(BiO)_2CO_3$ microspheres for efficient visible light photocatalysis. *ACS Catal.* 4: 4341–4350.

159 Xiong, T., Dong, X.a., Huang, H. et al. (2016). Single precursor mediated-synthesis of Bi semimetal deposited N-doped $(BiO)_2CO_3$ superstructures for highly promoted photocatalysis. *ACS Sustainable Chem. Eng.* 4: 2969–2979.

160 Zhai, Z.Y., Guo, X.N., Jin, G.Q., and Guo, X.Y. (2015). Visible light-induced selective photocatalytic aerobic oxidation of amines into imines on Cu/graphene. *Catal. Sci. Technol.* 5: 4202–4207.

161 Ni, Z.L., Zhang, W.D., Jiang, G.M. et al. (2017). Enhanced plasmonic photocatalysis by SiO_2@Bi microspheres with hot-electron transportation channels via Bi-O-Si linkages. *Chin. J. Catal.* 38: 1174–1183.

162 Ueno, K. and Misawa, H. (2013). Surface plasmon-enhanced photochemical reactions. *J. Photochem. Photobiol., C* 15: 31–52.

163 Linic, S., Christopher, P., and Ingram, D.B. (2011). Plasmonic-metal nanostructures for efficient conversion of solar to chemical energy. *Nat. Mater.* 10: 911–921.

164 Clavero, C. (2014). Plasmon-induced hot-electron generation at nanoparticle/metal-oxide interfaces for photovoltaic and photocatalytic devices. *Nat. Photonics* 8: 95–103.

165 Zhang, X.M., Chen, Y.L., Liu, R.S., and Tsai, D.P. (2013). Plasmonic photocatalysis. *Rep. Prog. Phys.* 76: 046401.

166 Long, R. and Prezhdo, O.V. (2014). Instantaneous generation of charge-separated state on TiO_2 surface sensitized with plasmonic nanoparticles. *J. Am. Chem. Soc.* 136: 4343–4354.

167 Cushing, S.K., Li, J., Meng, F. et al. (2012). Photocatalytic activity enhanced by plasmonic resonant energy transfer from metal to semiconductor. *J. Am. Chem. Soc.* 134: 15033–15041.

168 Ha, E., Lee, L.Y.S., Wang, J. et al. (2014). Significant enhancement in photocatalytic reduction of water to hydrogen by Au/Cu_2ZnSnS_4 nanostructure. *Adv. Mater.* 26: 3496–3500.

169 Jiang, R., Li, B., Fang, C., and Wang, J. (2014). Metal/semiconductor hybrid nanostructures for plasmon-enhanced applications. *Adv. Mater.* 26: 5274–5309.

170 Mo, Z., Xu, H., Chen, Z.G. et al. (2018). Gold/monolayer graphitic carbon nitride plasmonic photocatalyst for ultrafast electron transfer in solar-to-hydrogen energy conversion. *Chin. J. Catal.* 39: 760–770.

171 Li, Y.R., Guo, Y., Long, R. et al. (2018). Steering plasmonic hot electrons to realize enhanced full-spectrum photocatalytic hydrogen evolution. *Chin. J. Catal.* 39: 453–462.

172 Yang, X., Wang, Y., Xu, X. et al. (2017). Surface plasmon resonance-induced visible-light photocatalytic performance of silver/silver molybdate composites. *Chin. J. Catal.* 38: 260–269.

173 Yang, J.J., Liu, B.S., and Zhao, X.J. (2017). A visible-light-active $Au\text{-}Cu(I)@Na_2Ti_6O_{13}$ nanostructured hybrid pasmonic photocatalytic membrane for acetaldehyde elimination. *Chin. J. Catal.* 38: 2048–2055.

174 Warren, S.C. and Thimsen, E. (2012). Plasmonic solar water splitting. *Energy Environ. Sci.* 5: 5133–5146.

175 Creutz, C., Brunschwig, B.S., and Sutin, N. (2006). Interfacial charge-transfer absorption: 3. Application to semiconductor–molecule assemblies. *J. Phys. Chem. B* 110: 25181–25190.

176 Li, X., Yu, J., and Jaroniec, M. (2016). Hierarchical photocatalysts. *Chem. Soc. Rev.* 45: 2603–2636.

177 Wood, P.M. (1988). The potential diagram for oxygen at pH 7. *Biochem. J.* 253: 287–289.

178 Guan, L. and Chen, X. (2018). Photoexcited charge transport and accumulation in anatase TiO_2. *ACS Appl. Energy Mater.* 1: 4313–4320.

179 Zhang, J.Z. (2000). Interfacial charge carrier dynamics of colloidal semiconductor nanoparticles. *J. Phys. Chem. B* 104: 7239–7253.

180 Ravensbergen, J., Abdi, F.F., van Santen, J.H. et al. (2014). Unraveling the carrier dynamics of $BiVO_4$: a femtosecond to microsecond transient absorption study. *J. Phys. Chem. C* 118: 27793–27800.

181 Özgür, Ü., Alivov, Y.I., Liu, C. et al. (2005). A comprehensive review of ZnO materials and devices. *J. Appl. Phys.* 98: 041301.

182 Abdi, F.F., Savenije, T.J., May, M.M. et al. (2013). The origin of slow carrier transport in $BiVO_4$ thin film photoanodes: a time-resolved microwave conductivity study. *J. Phys. Chem. Lett.* 4: 2752–2757.

183 Zhang, J.F., Zhou, P., Liu, J.J., and Yu, J.G. (2014). New understanding of the difference of photocatalytic activity among anatase, rutile and brookite TiO_2. *Phys. Chem. Chem. Phys.* 16: 20382–20386.

184 Zhang, J., Wageh, S., Al-Ghamdi, A., and Yu, J. (2016). New understanding on the different photocatalytic activity of wurtzite and zinc-blende CdS. *Appl. Catal., B* 192: 101–107.

185 Li, X., Xie, J., Jiang, C. et al. (2018). Review on design and evaluation of environmental photocatalysts. *Front. Environ. Sci. Eng.* 12: 14.

186 He, R.A., Xu, D.F., Cheng, B. et al. (2018). Review on nanoscale Bi-based photocatalysts. *Nanoscale Horiz.* 3: 464–504.

187 Chen, S.Y. and Wang, L.W. (2012). Thermodynamic oxidation and reduction potentials of photocatalytic semiconductors in aqueous solution. *Chem. Mater.* 24: 3659–3666.

188 Yang, X., Cui, H., Li, Y. et al. (2013). Fabrication of Ag_3PO_4-graphene composites with highly efficient and stable visible light photocatalytic performance. *ACS Catal.* 3: 363–369.

189 Zhang, D., Tang, H., Wang, Y. et al. (2014). Synthesis and characterization of graphene oxide modified AgBr nanocomposites with enhanced photocatalytic activity and stability under visible light. *Appl. Surf. Sci.* 319: 306–311.

190 Li, J., Wei, L., Yu, C. et al. (2015). Preparation and characterization of graphene oxide/Ag_2CO_3 photocatalyst and its visible light photocatalytic activity. *Appl. Surf. Sci.* 358: 168–174.

191 Reddy, D.A., Lee, S., Choi, J. et al. (2015). Green synthesis of AgI-reduced graphene oxide nanocomposites: toward enhanced visible-light photocatalytic activity for organic dye removal. *Appl. Surf. Sci.* 341: 175–184.

192 Kudo, A. and Miseki, Y. (2009). Heterogeneous photocatalyst materials for water splitting. *Chem. Soc. Rev.* 38: 253–278.

193 Paracchino, A., Laporte, V., Sivula, K. et al. (2011). Highly active oxide photocathode for photoelectrochemical water reduction. *Nat. Mater.* 10: 456–461.

194 Gu, J., Yan, Y., Krizan, J.W. et al. (2014). *p*-Type $CuRhO_2$ as a self-healing photoelectrode for water reduction under visible light. *J. Am. Chem. Soc.* 136: 830–833.

195 Park, J.E., Hu, Y., Krizan, J.W. et al. (2018). Stable hydrogen evolution from an $AgRhO_2$ photocathode under visible light. *Chem. Mater.* 30: 2574–2582.

196 Di, T., Zhu, B., Zhang, J. et al. (2016). Enhanced photocatalytic H_2 production on CdS nanorod using cobalt-phosphate as oxidation cocatalyst. *Appl. Surf. Sci.* 389: 775–782.

197 Chen, S.S., Shen, S., Liu, G.J. et al. (2015). Interface engineering of a CoO_x/Ta_3N_5 photocatalyst for unprecedented water oxidation performance under visible-light-irradiation. *Angew. Chem. Int. Ed.* 54: 3047–3051.

198 Wang, P., Xia, Y., Wu, P. et al. (2014). Cu(II) as a general cocatalyst for improved visible-light photocatalytic performance of photosensitive Ag-based compounds. *J. Phys. Chem. C* 118: 8891–8898.

199 Wang, X., Wang, K., Feng, K. et al. (2014). Greatly enhanced photocatalytic activity of $TiO_{2-x}N_x$ by a simple surface modification of Fe(III) cocatalyst. *J. Mol. Catal. A: Chem.* 391: 92–98.

200 Yu, H., Xu, L., Wang, P. et al. (2014). Enhanced photoinduced stability and photocatalytic activity of AgBr photocatalyst by surface modification of Fe(III) cocatalyst. *Appl. Catal., B* 144: 75–82.

201 Peng, Y., Ji, J., and Chen, D. (2015). Ultrasound assisted synthesis of ZnO/reduced graphene oxide composites with enhanced photocatalytic activity and anti-photocorrosion. *Appl. Surf. Sci.* 356: 762–768.

202 Huang, M., Yu, J., Deng, C. et al. (2016). 3D nanospherical $Cd_xZn_{1-x}S$/reduced graphene oxide composites with superior photocatalytic activity and photocorrosion resistance. *Appl. Surf. Sci.* 365: 227–239.

203 Chen, J., Zhang, F., Zhao, Y.L. et al. (2016). Facile synthesis of CdS/C core-shell nanospheres with ultrathin carbon layer for enhanced photocatalytic properties and stability. *Appl. Surf. Sci.* 362: 126–131.

204 Cai, L., Xiong, X., Liang, N., and Long, Q. (2015). Highly effective and stable Ag_3PO_4-WO_3/MWCNTs photocatalysts for simultaneous Cr(VI) reduction and orange II degradation under visible light irradiation. *Appl. Surf. Sci.* 353: 939–948.

205 Wang, H., Li, J., Huo, P. et al. (2016). Preparation of Ag_2O/Ag_2CO_3/MWNTs composite photocatalysts for enhancement of ciprofloxacin degradation. *Appl. Surf. Sci.* 366: 1–8.

206 Miao, J., Xie, A., Li, S. et al. (2016). A novel reducing graphene/polyaniline/cuprous oxide composite hydrogel with unexpected photocatalytic activity for the degradation of Congo red. *Appl. Surf. Sci.* 360: 594–600.

207 Xu, X., Gao, Z., Cui, Z. et al. (2016). Synthesis of Cu_2O Octadecahedron/TiO_2 quantum dot heterojunctions with high visible light photocatalytic activity and high stability. *ACS Appl. Mater. Interfaces* 8: 91–101.

208 Liu, Y., Zhang, B., Luo, L. et al. (2015). TiO_2/Cu_2O Core/ultrathin shell nanorods as efficient and stable photocatalysts for water reduction. *Angew. Chem. Int. Ed.* 54: 15260–15265.

209 Liu, L., Yang, W., Sun, W. et al. (2015). Creation of $Cu_2O@TiO_2$ composite photocatalysts with *p–n* heterojunctions formed on exposed Cu_2O facets, their energy band alignment study, and their enhanced photocatalytic activity under illumination with visible light. *ACS Appl. Mater. Interfaces* 7: 1465–1476.

210 Liu, J., Wen, M., Chen, H. et al. (2014). Assembly of TiO_2-on-Cu_2O nanocubes with narrow-band Cu_2O-induced visible-light-enhanced photocatalytic activity. *ChemPlusChem* 79: 298–303.

211 Lalitha, K., Sadanandam, G., Kumari, V.D. et al. (2010). Highly stabilized and finely dispersed Cu_2O/TiO_2: a promising visible sensitive photocatalyst for continuous production of hydrogen from glycerol: water mixtures. *J. Phys. Chem. C* 114: 22181–22189.

212 Beigi, A.A., Fatemi, S., and Salehi, Z. (2014). Synthesis of nanocomposite CdS/TiO_2 and investigation of its photocatalytic activity for CO_2 reduction to CO and CH_4 under visible light irradiation. *J. CO_2 Util.* 7: 23–29.

213 Xiao, F.X., Miao, J., Wang, H.Y., and Liu, B. (2013). Self-assembly of hierarchically ordered CdS quantum dots-TiO_2 nanotube array heterostructures as efficient visible light photocatalysts for photoredox applications. *J. Mater. Chem. A* 1: 12229–12238.

214 Tian, F., Hou, D., Hu, F. et al. (2017). Pouous TiO_2 nanofibers decorated CdS nanoparticles by SILAR method for enhanced visible-light-driven photocatalytic activity. *Appl. Surf. Sci.* 391: 295–302.

215 Yang, G., Yang, B., Xiao, T., and Yan, Z. (2013). One-step solvothermal synthesis of hierarchically porous nanostructured CdS/TiO_2 heterojunction with higher visible light photocatalytic activity. *Appl. Surf. Sci.* 283: 402–410.

216 Fujishima, M., Nakabayashi, Y., Takayama, K. et al. (2016). High coverage formation of CdS quantum dots on TiO_2 by the photocatalytic growth of preformed seeds. *J. Phys. Chem. C* 120: 17365–17371.

217 Pan, X. and Xu, Y.J. (2015). Graphene-templated bottom-up fabrication of ultralarge binary CdS-TiO_2 nanosheets for photocatalytic selective reduction. *J. Phys. Chem. C* 119: 7184–7194.

218 Ma, K., Yehezkeli, O., Domaille, D.W. et al. (2015). Enhanced hydrogen production from DNA-assembled Z-scheme TiO_2-CdS photocatalyst systems. *Angew. Chem. Int. Ed.* 54: 11490–11494.

219 Wei, Y., Jiao, J., Zhao, Z. et al. (2015). Fabrication of inverse opal TiO_2-supported Au@CdS core-shell nanoparticles for efficient photocatalytic CO_2 conversion. *Appl. Catal., B* 179: 422–432.

220 Wei, Y., Jiao, J., Zhao, Z. et al. (2015). 3D ordered macroporous TiO_2-supported Pt@CdS core-shell nanoparticles: design, synthesis and efficient photocatalytic conversion of CO_2 with water to methane. *J. Mater. Chem. A* 3: 11074–11085.

221 Dong, W., Pan, F., Xu, L. et al. (2015). Facile synthesis of CdS@TiO_2 core-shell nanorods with controllable shell thickness and enhanced photocatalytic activity under visible light irradiation. *Appl. Surf. Sci.* 349: 279–286.

222 Liu, S., Zhang, N., Tang, Z.R., and Xu, Y.J. (2012). Synthesis of one-dimensional CdS@TiO_2 core-shell nanocomposites photocatalyst for selective redox: the dual role of TiO_2 shell. *ACS Appl. Mater. Interfaces* 4: 6378–6385.

223 Butburee, T., Bai, Y., Pan, J. et al. (2014). Step-wise controlled growth of metal@TiO_2 core-shells with plasmonic hot spots and their photocatalytic properties. *J. Mater. Chem. A* 2: 12776–12784.

224 Tanaka, A., Fuku, K., Nishi, T. et al. (2013). Functionalization of Au/TiO_2 plasmonic photocatalysts with Pd by formation of a core-shell structure for effective dechlorination of chlorobenzene under irradiation of visible light. *J. Phys. Chem. C* 117: 16983–16989.

225 Wu, X.F., Song, H.Y., Yoon, J.M. et al. (2009). Synthesis of core-shell Au@TiO_2 nanoparticles with truncated wedge-shaped morphology and their photocatalytic properties. *Langmuir* 25: 6438–6447.

226 Ji, L., McDaniel, M.D., Wang, S.J. et al. (2015). A silicon-based photocathode for water reduction with an epitaxial $SrTiO_3$ protection layer and a nanostructured catalyst. *Nat. Nanotechnol.* 10: 84–90.

227 Yu, H., Chen, F., Chen, F., and Wang, X. (2015). In situ self-transformation synthesis of g-C_3N_4-modified CdS heterostructure with enhanced photocatalytic activity. *Appl. Surf. Sci.* 358: 385–392.

228 Liu, L., Qi, Y., Hu, J. et al. (2015). Efficient visible-light photocatalytic hydrogen evolution and enhanced photostability of core@shell Cu_2O@g-C_3N_4 octahedra. *Appl. Surf. Sci.* 351: 1146–1154.

229 Zhang, J., Wang, Y., Jin, J. et al. (2013). Efficient visible-light photocatalytic hydrogen evolution and enhanced photostability of core/shell CdS/g-C_3N_4 nanowires. *ACS Appl. Mater. Interfaces* 5: 10317–10324.

230 Le Formal, F., Tetreault, N., Cornuz, M. et al. (2011). Passivating surface states on water splitting hematite photoanodes with alumina overlayers. *Chem. Sci.* 2: 737–743.

231 Song, G., Xin, F., Chen, J., and Yin, X. (2014). Photocatalytic reduction of CO_2 in cyclohexanol on CdS-TiO_2 heterostructured photocatalyst. *Appl. Catal., A* 473: 90–95.

232 Zhai, J., Tao, X., Pu, Y. et al. (2010). Core/shell structured ZnO/SiO_2 nanoparticles: preparation, characterization and photocatalytic property. *Appl. Surf. Sci.* 257: 393–397.

233 Chen, J.J., Wu, J.C.S., Wu, P.C., and Tsai, D.P. (2012). Improved photocatalytic activity of shell-isolated plasmonic photocatalyst Au@SiO_2/TiO_2 by promoted LSPR. *J. Phys. Chem. C* 116: 26535–26542.

234 Yoo, J.B., Yoo, H.J., Lim, B.W. et al. (2012). Controlled synthesis of monodisperse SiO_2-TiO_2 microspheres with a yolk-shell structure as effective photocatalysts. *ChemSusChem* 5: 2334–2340.

235 Zhang, X., Zhu, Y., Yang, X. et al. (2013). Enhanced visible light photocatalytic activity of interlayer-isolated triplex Ag@SiO_2@TiO_2 core-shell nanoparticles. *Nanoscale* 5: 3359–3366.

236 Yao, X. and Liu, X. (2014). One-pot synthesis of Ag/AgCl@SiO_2 core-shell plasmonic photocatalyst in natural geothermal water for efficient photocatalysis under visible light. *J. Mol. Catal. A: Chem.* 393: 30–38.

237 Nadrah, P., Gaberscek, M., and Sever Skapin, A. (2017). Selective degradation of model pollutants in the presence of core@shell TiO_2@SiO_2 photocatalyst. *Appl. Surf. Sci.* 405: 389–394.

238 Zhu, S. and Wang, D. (2017). Photocatalysis: basic principles, diverse forms of implementations and emerging scientific opportunities. *Adv. Energy Mater.* 7: 1700841.

239 Lian, Z., Xu, P., Wang, W. et al. (2015). C_{60}-Decorated CdS/TiO_2 mesoporous architectures with enhanced photostability and photocatalytic activity for H_2 evolution. *ACS Appl. Mater. Interfaces* 7: 4533–4540.

240 Luo, G., Jiang, X., Li, M. et al. (2013). Facile fabrication and enhanced photocatalytic performance of Ag/AgCl/rGO heterostructure photocatalyst. *ACS Appl. Mater. Interfaces* 5: 2161–2168.

241 Tong, R., Liu, C., Xu, Z. et al. (2016). Efficiently enhancing visible light photocatalytic activity of faceted TiO_2 nanocrystals by synergistic effects of core-shell structured Au@CdS nanoparticles and their selective deposition. *ACS Appl. Mater. Interfaces* 8: 21326–21333.

242 Hu, Z. and Yu, J.C. (2013). Pt_3Co-loaded CdS and TiO_2 for photocatalytic hydrogen evolution from water. *J. Mater. Chem. A* 1: 12221–12228.

243 Liu, S., Yang, M.Q., and Xu, Y.J. (2014). Surface charge promotes the synthesis of large, flat structured graphene-(CdS nanowire)-TiO_2 nanocomposites as versatile visible light photocatalysts. *J. Mater. Chem. A* 2: 430–440.

244 Wang, P., Ming, T., Wang, G. et al. (2014). Cocatalyst modification and nanonization of Ag/AgCl photocatalyst with enhanced photocatalytic performance. *J. Mol. Catal. A: Chem.* 381: 114–119.

245 Park, H., Kirn, Y.K., and Choi, W. (2011). Reversing CdS preparation order and its effects on photocatalytic hydrogen production of CdS/Pt-TiO_2 hybrids under visible light. *J. Phys. Chem. C* 115: 6141–6148.

246 Osterloh, F.E. (2007). Inorganic materials as catalysts for photochemical splitting of water. *Chem. Mater.* 20: 35–54.

247 Kumar, S.G. and Rao, K.S.R.K. (2017). Comparison of modification strategies towards enhanced charge carrier separation and photocatalytic degradation activity of metal oxide semiconductors (TiO_2, WO_3 and ZnO). *Appl. Surf. Sci.* 391: 124–148.

248 Bai, S., Jiang, J., Zhang, Q., and Xiong, Y. (2015). Steering charge kinetics in photocatalysis: intersection of materials syntheses, characterization techniques and theoretical simulations. *Chem. Soc. Rev.* 44: 2893–2939.

249 Bai, S., Jiang, W., Li, Z., and Xiong, Y. (2015). Surface and interface engineering in photocatalysis. *ChemNanoMat* 1: 223–239.

250 Zhang, P., Wang, T., Chang, X., and Gong, J. (2016). Effective charge carrier utilization in photocatalytic conversions. *Acc. Chem. Res.* 49: 911–921.

251 Devi, L.G. and Kavitha, R. (2016). A review on plasmonic metal-TiO_2 composite for generation, trapping, storing and dynamic vectorial transfer of photogenerated electrons across the Schottky junction in a photocatalytic system. *Appl. Surf. Sci.* 360: 601–622.

252 Song, S., Cheng, B., Wu, N. et al. (2016). Structure effect of graphene on the photocatalytic performance of plasmonic Ag/Ag_2CO_3-rGO for photocatalytic elimination of pollutants. *Appl. Catal., B* 181: 71–78.

253 Qi, L., Yu, J., Liu, G., and Wong, P.K. (2014). Synthesis and photocatalytic activity of plasmonic Ag@AgCl composite immobilized on titanate nanowire films. *Catal. Today* 224: 193–199.

254 Zhou, X., Liu, G., Yu, J., and Fan, W. (2012). Surface plasmon resonance-mediated photocatalysis by noble metal-based composites under visible light. *J. Mater. Chem.* 22: 21337–21354.

255 Wang, X., Li, S., Ma, Y. et al. (2011). H_2WO_4 center dot H_2O/Ag/AgCl composite nanoplates: a plasmonic Z-scheme visible-light photocatalyst. *J. Phys. Chem. C* 115: 14648–14655.

256 Low, J., Yu, J., Li, Q., and Cheng, B. (2014). Enhanced visible-light photocatalytic activity of plasmonic Ag and graphene co-modified Bi_2WO_6 nanosheets. *Phys. Chem. Chem. Phys.* 16: 1111–1120.

257 Jiang, J., Yu, J., and Cao, S. (2016). Au/PtO nanoparticle-modified g-C_3N_4 for plasmon-enhanced photocatalytic hydrogen evolution under visible light. *J. Colloid Interface Sci.* 461: 56–63.

258 Yu, S., Wilson, A.J., Kumari, G. et al. (2017). Opportunities and challenges of solar-energy-driven carbon dioxide to fuel conversion with plasmonic catalysts. *ACS Energy Lett.* 2: 2058–2070.

259 Madhusudan, P., Zhang, J., Yu, J. et al. (2016). One-pot template-free synthesis of porous $CdMoO_4$ microspheres and their enhanced photocatalytic activity. *Appl. Surf. Sci.* 387: 202–213.

260 Lei, C.S., Zhu, X.F., Zhu, B.C. et al. (2017). Superb adsorption capacity of hierarchical calcined Ni/Mg/Al layered double hydroxides for Congo red and Cr(VI) ions. *J. Hazard. Mater.* 321: 801–811.

261 Lei, C., Zhu, X., Zhu, B. et al. (2016). Hierarchical NiO-SiO_2 composite hollow microspheres with enhanced adsorption affinity towards Congo red in water. *J. Colloid Interface Sci.* 466: 238–246.

262 He, R., Zhang, J., Yu, J., and Cao, S. (2016). Room-temperature synthesis of BiOI with tailorable (0 0 1) facets and enhanced photocatalytic activity. *J. Colloid Interface Sci.* 478: 201–208.

263 Chen, F., Liu, S.W., and Yu, J.G. (2016). Efficient removal of gaseous formaldehyde in air using hierarchical titanate nanospheres with in situ amine functionalization. *Phys. Chem. Chem. Phys.* 18: 18161–18168.

264 He, R., Cao, S., Yu, J., and Yang, Y. (2016). Microwave-assisted solvothermal synthesis of $Bi_4O_5I_2$ hierarchical architectures with high photocatalytic performance. *Catal. Today* 264: 221–228.

265 Chen, M., Huang, Y., and Lee, S.C. (2017). Salt-assisted synthesis of hollow Bi_2WO_6 microspheres with superior photocatalytic activity for NO removal. *Chin. J. Catal.* 38: 348–356.

266 Yang, J., Wang, D., Han, H., and Li, C. (2013). Roles of cocatalysts in photocatalysis and photoelectrocatalysis. *Acc. Chem. Res.* 46: 1900–1909.

267 Ran, J., Zhang, J., Yu, J. et al. (2014). Earth-abundant cocatalysts for semiconductor-based photocatalytic water splitting. *Chem. Soc. Rev.* 43: 7787–7812.

268 Yu, J., Zhang, J., and Liu, S. (2010). Ion-exchange synthesis and enhanced visible-light photoactivity of CuS/ZnS nanocomposite hollow spheres. *J. Phys. Chem. C* 114: 13642–13649.

269 Ran, J., Yu, J., and Jaroniec, M. (2011). $Ni(OH)_2$ modified CdS nanorods for highly efficient visible-light-driven photocatalytic H_2 generation. *Green Chem.* 13: 2708–2713.

270 Chen, W., Chu, M., Gao, L. et al. (2015). $Ni(OH)_2$ loaded on TaON for enhancing photocatalytic water splitting activity under visible light irradiation. *Appl. Surf. Sci.* 324: 432–437.

271 Xu, Y. and Xu, R. (2015). Nickel-based cocatalysts for photocatalytic hydrogen production. *Appl. Surf. Sci.* 351: 779–793.

272 Zou, X. and Zhang, Y. (2015). Noble metal-free hydrogen evolution catalysts for water splitting. *Chem. Soc. Rev.* 44: 5148–5180.

273 Zhou, X., Jin, J., Zhu, X.J. et al. (2016). New $Co(OH)_2$/CdS nanowires for efficient visible light photocatalytic hydrogen production. *J. Mater. Chem. A* 4: 5282–5287.

274 Chai, B., Liu, C., Wang, C.L. et al. (2017). Photocatalytic hydrogen evolution activity over $MoS_2/ZnIn_2S_4$ microspheres. *Chin. J. Catal.* 38: 2067–2075.

275 Chen, F., Yang, H., Wang, X., and Yu, H. (2017). Facile synthesis and enhanced photocatalytic H_2-evolution performance of NiS_2-modified g-C_3N_4 photocatalysts. *Chin. J. Catal.* 38: 296–304.

276 He, K., Xie, J., Yang, Z. et al. (2017). Earth-abundant WC nanoparticles as an active noble-metal-free cocatalyst for highly boosted photocatalytic H_2 production over g-C_3N_4 nanosheets under visible light. *Catal. Sci. Technol.* 7: 1193–1202.

277 Jiang, D.C., Zhu, L., Irfan, R.M. et al. (2017). Integrating noble-metal-free NiS cocatalyst with a semiconductor heterojunction composite for efficient photocatalytic H_2 production in water under visible light. *Chin. J. Catal.* 38: 2102–2109.

278 Liu, C., Zhang, Y., Dong, F. et al. (2017). Chlorine intercalation in graphitic carbon nitride for efficient photocatalysis. *Appl. Catal., B* 203: 465–474.

279 Ma, S., Xu, X.M., Xie, J., and Li, X. (2017). Improved visible-light photocatalytic H_2 generation over CdS nanosheets decorated by NiS_2 and metallic carbon black as dual earth-abundant cocatalysts. *Chin. J. Catal.* 38: 1970–1980.

280 Wen, J., Xie, J., Shen, R. et al. (2017). Markedly enhanced visible-light photocatalytic H_2 generation over g-C_3N_4 nanosheets decorated by robust nickel phosphide ($Ni_{12}P_5$) cocatalysts. *Dalton Trans.* 46: 1794–1802.

281 Xu, W.C. and Wang, H.X. (2017). Earth-abundant amorphous catalysts for electrolysis of water. *Chin. J. Catal.* 38: 991–1005.

282 Liang, Q.S., Shi, F.B., Xiao, X.F. et al. (2018). In situ growth of CoP nanoparticles anchored on black phosphorus nanosheets for enhanced photocatalytic hydrogen production. *ChemCatChem* 10: 2179–2183.

283 Ma, B.J., Zhang, R.S., Lin, K.Y. et al. (2018). Large-scale synthesis of noble-metal-free phosphide/CdS composite photocatalysts for enhanced H_2 evolution under visible light irradiation. *Chin. J. Catal.* 39: 527–533.

284 Wang, Q.Z., Niu, T.J., Wang, L. et al. (2018). NiFe layered double-hydroxide nanoparticles for efficiently enhancing performance of $BiVO_4$ photoanode in photoelectrochemical water splitting. *Chin. J. Catal.* 39: 613–618.

285 Low, J., Yu, J., and Ho, W. (2015). Graphene-based photocatalysts for CO_2 reduction to solar fuel. *J. Phys. Chem. Lett.* 6: 4244–4251.

286 Cao, S. and Yu, J. (2016). Carbon-based H_2-production photocatalytic materials. *J. Photochem. Photobiol., C* 27: 72–99.

287 Low, J., Yu, J., Jaroniec, M. et al. (2017). Heterojunction photocatalysts. *Adv. Mater.*: 1601694.

288 Moniz, S.J.A., Shevlin, S.A., Martin, D.J. et al. (2015). Visible-light driven heterojunction photocatalysts for water splitting – a critical review. *Energy Environ. Sci.* 8: 731–759.

289 Wang, H., Zhang, L., Chen, Z. et al. (2014). Semiconductor heterojunction photocatalysts: design, construction, and photocatalytic performances. *Chem. Soc. Rev.* 43: 5234–5244.

290 Fu, J.W., Yu, J.G., Jiang, C.J., and Cheng, B. (2018). g-C_3N_4-Based heterostructured photocatalysts. *Adv. Energy Mater.* 8: 1701503.

291 Du, H., Liu, Y.N., Shen, C.C., and Xu, A.W. (2017). Nanoheterostructured photocatalysts for improving photocatalytic hydrogen production. *Chin. J. Catal.* 38: 1295–1306.

292 Zhang, Z., Huang, Y., Liu, K. et al. (2015). Multichannel-improved charge-carrier dynamics in well-designed hetero-nanostructural plasmonic photocatalysts toward highly efficient solar-to-fuels conversion. *Adv. Mater.* 27: 5906–5914.

293 Zhao, Y., Huang, X., Tan, X. et al. (2016). Fabrication of BiOBr nanosheets@TiO_2 nanobelts *p–n* junction photocatalysts for enhanced visible-light activity. *Appl. Surf. Sci.* 365: 209–217.

294 Yang, S., Xu, D., Chen, B. et al. (2016). Synthesis and visible-light-driven photocatalytic activity of *p–n* heterojunction Ag_2O/$NaTaO_3$ nanocubes. *Appl. Surf. Sci.* 383: 214–221.

295 Sun, B., Zhou, G., Gao, T. et al. (2016). NiO nanosheet/TiO_2 nanorod-constructed *p–n* heterostructures for improved photocatalytic activity. *Appl. Surf. Sci.* 364: 322–331.

296 Li, Y., Wang, B., Liu, S. et al. (2015). Synthesis and characterization of Cu_2O/TiO_2 photocatalysts for H_2 evolution from aqueous solution with different scavengers. *Appl. Surf. Sci.* 324: 736–744.

297 Duo, F., Wang, Y., Mao, X. et al. (2015). A $BiPO_4$/BiOCl heterojunction photocatalyst with enhanced electron-hole separation and excellent photocatalytic performance. *Appl. Surf. Sci.* 340: 35–42.

298 Tian, N., Huang, H., and Zhang, Y. (2015). Mixed-calcination synthesis of $CdWO_4$/g-C_3N_4 heterojunction with enhanced visible-light-driven photocatalytic activity. *Appl. Surf. Sci.* 358: 343–349.

299 Feng, Y., Yan, X., Liu, C. et al. (2015). Hydrothermal synthesis of CdS/Bi_2MoO_6 heterojunction photocatalysts with excellent visible-light-driven photocatalytic performance. *Appl. Surf. Sci.* 353: 87–94.

300 Cao, C., Xiao, L., Chen, C., and Cao, Q. (2015). Synthesis of novel Cu_2O/BiOCl heterojunction nanocomposites and their enhanced photocatalytic activity under visible light. *Appl. Surf. Sci.* 357: 1171–1179.

301 Guo, X., Chen, Y.B., Qin, Z.X. et al. (2018). Facet-selective growth of cadmium sulfide nanorods on zinc oxide microrods: intergrowth effect for improved photocatalytic performance. *ChemCatChem* 10: 153–158.

302 Wang, B., Zhang, J.T., and Huang, F. (2017). Enhanced visible light photocatalytic H_2 evolution of metal-free g-C_3N_4/SiC heterostructured photocatalysts. *Appl. Surf. Sci.* 391: 449–456.

303 Teng, W., Tan, X.J., Li, X.Y., and Tang, Y.B. (2017). Novel Ag_3PO_4/MoO_3 *p–n* heterojunction with enhanced photocatalytic activity and stability under visible light irradiation. *Appl. Surf. Sci.* 409: 250–260.

304 Li, P., Zhou, Y., Zhao, Z. et al. (2015). Hexahedron prism-anchored octahedronal CeO_2: crystal facet-based homojunction promoting efficient solar fuel synthesis. *J. Am. Chem. Soc.* 137: 9547–9550.

305 Jiang, G., Wei, M., Yuan, S., and Chang, Q. (2016). Efficient photocatalytic reductive dechlorination of 4-chlorophenol to phenol on {001}/{101} facets co-exposed TiO_2 nanocrystals. *Appl. Surf. Sci.* 362: 418–426.

306 Huang, M., Yu, J., Hu, Q. et al. (2016). Preparation and enhanced photocatalytic activity of carbon nitride/titania(001 vs 101 facets)/reduced graphene oxide(g-C_3N_4/TiO_2/rGO) hybrids under visible light. *Appl. Surf. Sci.* 389: 1084–1093.

307 Lu, D., Zhang, G., and Wan, Z. (2015). Visible-light-driven g-C_3N_4/Ti^{3+}-TiO_2 photocatalyst co-exposed {001} and {101} facets and its enhanced photocatalytic activities for organic pollutant degradation and Cr(VI) reduction. *Appl. Surf. Sci.* 358: 223–230.

308 Zhang, J., Zhang, L.L., Shi, Y.X. et al. (2017). Anatase TiO_2 nanosheets with coexposed {101} and {001} facets coupled with ultrathin SnS_2 nanosheets as a face-to-face *n-p-n* dual heterojunction photocatalyst for enhancing photocatalytic activity. *Appl. Surf. Sci.* 420: 839–848.

309 Xia, P.F., Zhu, B.C., Cheng, B. et al. (2018). 2D/2D g-C_3N_4/MnO_2 nanocomposite as a direct Z-scheme photocatalyst for enhanced photocatalytic activity. *ACS Sustainable Chem. Eng.* 6: 965–973.

310 Lv, J.L., Zhang, J.F., Liu, J. et al. (2018). Bi SPR-promoted Z-scheme Bi_2MoO_6/CdS-diethylenetriamine composite with effectively enhanced visible light photocatalytic hydrogen evolution activity and stability. *ACS Sustainable Chem. Eng.* 6: 696–706.

311 Xu, Q., Zhu, B., Jiang, C. et al. (2018). Constructing 2D/2D Fe_2O_3/g-C_3N_4 direct Z-scheme photocatalysts with enhanced H_2 generation performance. *Sol. RRL* 2: 1800006.

312 Tang, H., Fu, Y., Chang, S. et al. (2017). Construction of Ag_3PO_4/Ag_2MoO_4 Z-scheme heterogeneous photocatalyst for the remediation of organic pollutants. *Chin. J. Catal.* 38: 337–347.

313 Fu, Y.H., Li, Z.J., Liu, Q.Q. et al. (2017). Construction of carbon nitride and MoS_2 quantum dot 2D/0D hybrid photocatalyst: direct Z-scheme mechanism for improved photocatalytic activity. *Chin. J. Catal.* 38: 2160–2170.

314 Song, S., Meng, A., Jiang, S. et al. (2017). Construction of Z-scheme Ag_2CO_3/N-doped graphene photocatalysts with enhanced visible-light photocatalytic activity by tuning the nitrogen species. *Appl. Surf. Sci.* 396: 1368–1374.

315 Ma, Y.J., Bian, Y., Liu, Y. et al. (2018). Construction of Z-scheme system for enhanced photocatalytic H_2 evolution based on CdS quantum dots/CeO_2 nanorods heterojunction. *ACS Sustainable Chem. Eng.* 6: 2552–2562.

316 Yu, W., Chen, J., Shang, T. et al. (2017). Direct Z-scheme g-C_3N_4/WO_3 photocatalyst with atomically defined junction for H_2 production. *Appl. Catal., B* 219: 693–704.

317 Meng, A.Y., Zhu, B.C., Zhong, B. et al. (2017). Direct Z-scheme TiO_2/CdS hierarchical photocatalyst for enhanced photocatalytic H_2-production activity. *Appl. Surf. Sci.* 422: 518–527.

318 Xu, F.Y., Zhang, L.Y., Cheng, B., and Yu, J.G. (2018). Direct Z-scheme TiO_2/NiS core-shell hybrid nanofibers with enhanced photocatalytic H_2-production activity. *ACS Sustainable Chem. Eng.* 6: 12291–12298.

319 Li, J., Zhang, M., Li, Q., and Yang, J. (2017). Enhanced visible light activity on direct contact Z-scheme g-C_3N_4-TiO_2 photocatalyst. *Appl. Surf. Sci.* 391: 184–193.

320 Zhu, C., Zhang, L., Jiang, B. et al. (2016). Fabrication of Z-scheme Ag_3PO_4/MoS_2 composites with enhanced photocatalytic activity and stability for organic pollutant degradation. *Appl. Surf. Sci.* 377: 99–108.

321 Hu, T.P., Li, P.F., Zhang, J.F. et al. (2018). Highly efficient direct Z-scheme WO3/CdS-diethylenetriamine photocatalyst and its enhanced photocatalytic H_2 evolution under visible light irradiation. *Appl. Surf. Sci.* 442: 20–29.

322 Lu, D.Z., Wang, H.M., Zhao, X.N. et al. (2017). Highly efficient visible-light-induced photoactivity of Z-scheme g-C_3N_4/Ag/MoS_2 ternary photocatalysts for organic pollutant degradation and production of hydrogen. *ACS Sustainable Chem. Eng.* 5: 1436–1445.

323 Pan, L., Zhang, J., Jia, X. et al. (2017). Highly efficient Z-scheme WO_{3-x} quantum dots/TiO_2 for photocatalytic hydrogen generation. *Chin. J. Catal.* 38: 253–259.

324 Li, J., Yuan, H., and Zhu, Z. (2016). Improved photoelectrochemical performance of Z-scheme g-C_3N_4/Bi_2O_3/$BiPO_4$ heterostructure and degradation property. *Appl. Surf. Sci.* 385: 34–41.

325 Cui, M., Yu, J., Lin, H. et al. (2016). In-situ preparation of Z-scheme AgI/Bi_5O_7I hybrid and its excellent photocatalytic activity. *Appl. Surf. Sci.* 387: 912–920.

326 Hu, J.Y., Zhang, S.S., Cao, Y.H. et al. (2018). Novel highly active anatase/rutile TiO_2 photocatalyst with hydrogenated heterophase interface structures for photoelectrochemical water splitting into hydrogen. *ACS Sustainable Chem. Eng.* 6: 10823–10832.

327 Luo, J., Zhou, X., Ma, L., and Xu, X. (2016). Rational construction of Z-scheme Ag_2CrO_4/g-C_3N_4 composites with enhanced visible-light photocatalytic activity. *Appl. Surf. Sci.* 390: 357–367.

328 He, R.A., Zhou, J.Q., Fu, H.Q. et al. (2018). Room-temperature in situ fabrication of Bi_2O_3/g-C_3N_4 direct Z-scheme photocatalyst with enhanced photocatalytic activity. *Appl. Surf. Sci.* 430: 273–282.

329 Xin, L., Jin, A.L., Jia, Y.S. et al. (2017). Synergy of adsorption and visible-light photocatalytic degradation of methylene blue by a bifunctional Z-scheme heterojunction of WO_3/g-C_3N_4. *Appl. Surf. Sci.* 405: 359–371.

330 Ge, H.N., Xu, F.Y., Cheng, B. et al. (2019). S-Scheme heterojunction TiO_2/CdS nanocomposite nanofiber as H_2-production photocatalyst. *ChemCatChem* 11: 10.

331 Xu, Q.L., Zhang, L.Y., Yu, J.G. et al. (2018). Direct Z-scheme photocatalysts: principles, synthesis, and applications. *Mater. Today* 21: 1042–1063.

332 Di, T.M., Xu, Q.L., Ho, W.K. et al. (2019). Review on metal sulphide-based Z-scheme photocatalysts. *ChemCatChem* 11: 1394–1411.

333 Lee, J., Ye, H., Pan, S., and Bard, A.J. (2008). Screening of photocatalysts by scanning electrochemical microscopy. *Anal. Chem.* 80: 7445–7450.

334 Ye, H., Lee, J., Jang, J.S., and Bard, A.J. (2010). Rapid screening of $BiVO_4$-based photocatalysts by scanning electrochemical microscopy (SECM) and studies of their photoelectrochemical properties. *J. Phys. Chem. C* 114: 13322–13328.

335 Katz, J.E., Gingrich, T.R., Santori, E.A., and Lewis, N.S. (2009). Combinatorial synthesis and high-throughput photopotential and photocurrent screening of mixed-metal oxides for photoelectrochemical water splitting. *Energy Environ. Sci.* 2: 103–112.

336 Park, H.S., Kweon, K.E., Ye, H. et al. (2011). Factors in the metal doping of $BiVO_4$ for improved photoelectrocatalytic activity as studied by scanning electrochemical microscopy and first-principles density-functional calculation. *J. Phys. Chem. C* 115: 17870–17879.

337 Greeley, J., Jaramillo, T.F., Bonde, J. et al. (2006). Computational high-throughput screening of electrocatalytic materials for hydrogen evolution. *Nat. Mater.* 5: 909–913.

338 Ye, H., Park, H.S., and Bard, A.J. (2011). Screening of electrocatalysts for photoelectrochemical water oxidation on W-doped $BiVO_4$ photocatalysts by scanning electrochemical microscopy. *J. Phys. Chem. C* 115: 12464–12470.

339 Haber, J.A., Cai, Y., Jung, S. et al. (2014). Discovering Ce-rich oxygen evolution catalysts, from high throughput screening to water electrolysis. *Energy Environ. Sci.* 7: 682–688.

340 Xiang, C., Suram, S.K., Haber, J.A. et al. (2014). High-throughput bubble screening method for combinatorial discovery of electrocatalysts for water splitting. *ACS Comb. Sci.* 16: 47–52.

341 Yu, W., Zhang, J., and Peng, T. (2016). New insight into the enhanced photocatalytic activity of N-, C- and S-doped ZnO photocatalysts. *Appl. Catal., B* 181: 220–227.

342 Zhu, B., Zhang, J., Jiang, C. et al. (2017). First principle investigation of halogen-doped monolayer g-C_3N_4 photocatalyst. *Appl. Catal., B* 207: 27–34.

343 Zhang, X., Zhao, X., Wu, D. et al. (2016). $MnPSe_3$ monolayer: a promising 2D visible-light photohydrolytic catalyst with high carrier mobility. *Adv. Sci.* 3: 1600062.

344 Yan, Q., Yu, J., Suram, S.K. et al. (2017). Solar fuels photoanode materials discovery by integrating high-throughput theory and experiment. *Proc. Natl. Acad. Sci. U.S.A.* 114: 3040–3043.

345 Zhou, L., Yan, Q., Shinde, A. et al. (2015). High throughput discovery of solar fuels photoanodes in the CuO–V_2O_5 system. *Adv. Energy Mater.* 5: 1500968.

346 Bard, A. and Fox, M. (1995). Artificial photosynthesis: solar splitting of water to hydrogen and oxygen. *Acc. Chem. Res.* 28: 141–145.

347 Maeda, K. (2013). Z-Scheme water splitting using two different semiconductor photocatalysts. *ACS Catal.* 3: 1486–1503.

348 Sasaki, Y., Nemoto, H., Saito, K., and Kudo, A. (2009). Solar water splitting using powdered photocatalysts driven by Z-schematic interparticle electron transfer without an electron mediator. *J. Phys. Chem. C* 113: 17536–17542.

349 Zhang, L.J., Li, S., Liu, B.K. et al. (2014). Highly efficient CdS/WO_3 photocatalysts: Z-scheme photocatalytic mechanism for their enhanced photocatalytic H_2 evolution under visible light. *ACS Catal.* 4: 3724–3729.

350 Liu, H., Yuan, J., and Shangguan, W. (2006). Photochemical reduction and oxidation of water including sacrificial reagents and Pt/TiO_2 catalyst. *Energy Fuels* 20: 2289–2292.

351 Cheng, D., Negreiros, F.R., Aprà, E., and Fortunelli, A. (2013). Computational approaches to the chemical conversion of carbon dioxide. *ChemSusChem* 6: 944–965.

352 Li, X., Wen, J., Low, J. et al. (2014). Design and fabrication of semiconductor photocatalyst for photocatalytic reduction of CO_2 to solar fuel. *Sci. China Mater.* 57: 70–100.

353 Li, H., Lei, Y., Huang, Y. et al. (2011). Photocatalytic reduction of carbon dioxide to methanol by Cu_2O/SiC nanocrystallite under visible light irradiation. *J. Nat. Gas Chem.* 20: 145–150.

354 Li, X., Liu, H., Luo, D. et al. (2012). Adsorption of CO_2 on heterostructure CdS(Bi_2S_3)/TiO_2 nanotube photocatalysts and their photocatalytic activities in the reduction of CO_2 to methanol under visible light irradiation. *Chem. Eng. J.* 180: 151–158.

355 Yu, J., Wang, K., Xiao, W., and Cheng, B. (2014). Photocatalytic reduction of CO_2 into hydrocarbon solar fuels over g-C_3N_4-Pt nanocomposite photocatalysts. *Phys. Chem. Chem. Phys.* 16: 11492–11501.

356 Wang, K., Li, Q., Liu, B. et al. (2015). Sulfur-doped g-C_3N_4 with enhanced photocatalytic CO_2-reduction performance. *Appl. Catal. B: Environ.* 176–177: 44–52.

357 Liu, Y.Y., Huang, B.B., Dai, Y. et al. (2009). Selective ethanol formation from photocatalytic reduction of carbon dioxide in water with $BiVO_4$ photocatalyst. *Catal. Commun.* 11: 210–213.

358 Mao, J., Peng, T.Y., Zhang, X.H. et al. (2012). Selective methanol production from photocatalytic reduction of CO_2 on $BiVO_4$ under visible light irradiation. *Catal. Commun.* 28: 38–41.

359 Zhao, Y., Chen, G., Bian, T. et al. (2015). Defect-rich ultrathin ZnAl-layered double hydroxide nanosheets for efficient photoreduction of CO_2 to CO with water. *Adv. Mater.* 27: 7824–7831.

360 Zhang, Z., Wang, Z., Cao, S.W., and Xue, C. (2013). Au/Pt nanoparticle-decorated TiO_2 nanofibers with plasmon-enhanced photocatalytic activities for solar-to-fuel conversion. *J. Phys. Chem. C* 117: 25939–25947.

361 Xu, Q., Yu, J., Zhang, J. et al. (2015). Cubic anatase TiO_2 nanocrystals with enhanced photocatalytic CO_2 reduction activity. *Chem. Commun.* 51: 7950–7953.

362 Wang, W., Xu, D., Cheng, B. et al. (2017). Hybrid carbon@TiO_2 hollow spheres with enhanced photocatalytic CO_2 reduction activity. *J. Mater. Chem. A* 5: 5020–5029.

363 Huang, Q., Yu, J., Cao, S. et al. (2015). Efficient photocatalytic reduction of CO_2 by amine-functionalized g-C_3N_4. *Appl. Surf. Sci.* 358: 350–355.

364 Liu, S., Xia, J., and Yu, J. (2015). Amine-functionalized titanate nanosheet-assembled yolk@shell microspheres for efficient cocatalyst-free

visible-light photocatalytic CO_2 reduction. *ACS Appl. Mater. Interfaces* 7: 8166–8175.

365 Neatu, S., Macia-Agullo, J.A., Concepcion, P., and Garcia, H. (2014). Gold-copper nanoalloys supported on TiO_2 as photocatalysts for CO_2 reduction by water. *J. Am. Chem. Soc.* 136: 15969–15976.

366 Pastor, E., Pesci, F.M., Reynal, A. et al. (2014). Interfacial charge separation in Cu_2O/RuO_x as a visible light driven CO_2 reduction catalyst. *Phys. Chem. Chem. Phys.* 16: 5922–5926.

367 Tsai, C.W., Chen, H.M., Liu, R.S. et al. (2011). Ni@NiO core-shell structure-modified nitrogen-doped $InTaO_4$ for solar-driven highly efficient CO_2 reduction to methanol. *J. Phys. Chem. C* 115: 10180–10186.

368 Zhai, Q., Xie, S., Fan, W. et al. (2013). Photocatalytic conversion of carbon dioxide with water to methane: platinum and copper(I) oxide co-catalysts with a core-shell structure. *Angew. Chem. Int. Ed.* 52: 5776–5779.

369 Hamdy, M.S., Amrollahi, R., Sinev, I. et al. (2014). Strategies to design efficient silica-supported photocatalysts for reduction of CO_2. *J. Am. Chem. Soc.* 136: 594–597.

370 Hoffmann, M., Martin, S., Choi, W., and Bahnemann, D. (1995). Environmental applications of semiconductor photocatalysis. *Chem. Rev.* 95: 69–96.

371 Chen, C., Ma, W., and Zhao, J. (2010). Semiconductor-mediated photodegradation of pollutants under visible-light irradiation. *Chem. Soc. Rev.* 39: 4206–4219.

372 Park, H., Park, Y., Kim, W., and Choi, W. (2013). Surface modification of TiO_2 photocatalyst for environmental applications. *J. Photochem. Photobiol., C* 15: 1–20.

373 Chatterjee, D. and Dasgupta, S. (2005). Visible light induced photocatalytic degradation of organic pollutants. *J. Photochem. Photobiol., C* 6: 186–205.

374 Zhang, H., Chen, G., and Bahnemann, D.W. (2009). Photoelectrocatalytic materials for environmental applications. *J. Mater. Chem.* 19: 5089–5121.

375 Chong, M.N., Jin, B., Chow, C.W.K., and Saint, C. (2010). Recent developments in photocatalytic water treatment technology: a review. *Water Res.* 44: 2997–3027.

376 Zhao, B.X. and Zhang, P.Y. (2009). Photocatalytic decomposition of perfluorooctanoic acid with beta-Ga_2O_3 wide bandgap photocatalyst. *Catal. Commun.* 10: 1184–1187.

377 Li, X.Y., Zhang, P.Y., Jin, L. et al. (2012). Efficient photocatalytic decomposition of perfluorooctanoic acid by indium oxide and its mechanism. *Environ. Sci. Technol.* 46: 5528–5534.

378 Zhang, L., Ran, J., Qiao, S.Z., and Jaroniec, M. (2019). Characterization of semiconductor photocatalysts. *Chem. Soc. Rev.* 48: 5184–5206.